

## Conjugate strike-slip faulting along the Bangong-Nujiang suture zone accommodates coeval east-west extension and north-south shortening in the interior of the Tibetan Plateau

Michael Taylor,<sup>1</sup> An Yin,<sup>1</sup> Frederick J. Ryerson,<sup>2</sup> Paul Kapp,<sup>1,3</sup> and Lin Ding<sup>4</sup>

Received 25 January 2002; revised 13 January 2003; accepted 5 March 2003; published 28 August 2003.

[1] Geologic investigations of how the Tibetan plateau is currently deforming have focused primarily on its boundary faults. Consequently, how the interior of the plateau deforms remains poorly understood. To fill this gap in knowledge, we conducted field mapping, analysis of remote sensing and digital topographic data, and reinterpretation of existing geologic maps in central Tibet. This study reveals a 200–300 km wide and 1500–1800 km long east trending zone of conjugate strike-slip faults across central Tibet. The central Tibet conjugate fault zone is comprised of northeast striking left-slip faults north of the Bangong-Nujiang suture and northwest striking right-slip faults south of the suture zone. These strike-slip faults are kinematically linked with north trending Tibetan rifts located north and south of the conjugate fault systems. Without exception, all conjugate faults intersect or merge toward one another along the Bangong-Nujiang suture zone. Motion on these faults accommodates coeval east-west extension and north-south contraction. To determine the fault kinematics and the magnitude of fault slip, we investigated three conjugate fault sets in the central Tibet fault zone. These include from east to west, the Dong Co, Bue Co, and Aishi Co conjugate fault systems, which are adjacent to the Bangong-Nujiang suture zone and separated by a distance of 400 and 70 km, respectively. The average magnitude of fault motion on individual strike-slip faults is  $\sim 12$  km as determined by offsets of Tertiary thrusts and Paleozoic-Mesozoic lithologic units. The conjugate fault configuration requires  $\sim 12$  km of north-south contraction across the 200–300 km fault zone since its initiation. Because the conjugate strike-slip faults are

kinematically linked with the north trending Tibetan rifts which initiated between 14 and 8 Ma, our estimated magnitude of north-south contraction implies a contraction rate of  $\sim 1$ –2 mm/yr across central Tibet. The relatively closely spaced ( $<150$  km) basins may result from a series of conjugate strike-slip fault systems in the interior of Tibet. These structures likely formed by eastward spreading of the Tibetan crust via distributed eastward extrusion of small ( $<150$  km wide) wedge-shaped crustal blocks that leave a space at their trailing end. **INDEX TERMS:** 8107 Tectonophysics: Continental neotectonics; 8109 Tectonophysics: Continental tectonics—extensional (0905); 8005 Structural Geology: Folds and folding; 9320 Information Related to Geographic Region: Asia; 8010 Structural Geology: Fractures and faults; **KEYWORDS:** conjugate strike-slip faults, Tibet, neotectonics, extrusion tectonics. **Citation:** Taylor, M., A. Yin, F. J. Ryerson, P. Kapp, and L. Ding, Conjugate strike-slip faulting along the Bangong-Nujiang suture zone accommodates coeval east-west extension and north-south shortening in the interior of the Tibetan Plateau, *Tectonics*, 22(4), 1044, doi:10.1029/2002TC001361, 2003.

### 1. Introduction

[2] The classic debate about the Indo-Asian collision centers on how  $>1500$  km of northward penetration of India has been accommodated by intracontinental deformation in Asia. The lateral extrusion hypothesis emphasizes the role of large-scale strike-slip faults in transporting relatively undeformed continental blocks eastward away from the Indo-Asian convergent front [Peltzer and Tapponnier, 1988]. In contrast, the crustal thickening model suggests that indentation of India into Asia has been accommodated by distributed north-south shortening [Dewey and Burke, 1973]. The first hypothesis requires that the strike-slip faults be discrete and cut through the entire lithosphere with hundreds of kilometers of slip [Peltzer and Tapponnier, 1988; Avouac and Tapponnier, 1993]. Discrete deformation in extrusion tectonics also implies that major strike-slip faults in Asia move at rates of several cm/yr. The second hypothesis requires contractional structures such as thrusts and folds to be distributed throughout the collision zone with individual faults having much smaller magnitude of offsets ( $\ll 100$ s of kilometers) and moving at rates of less than a few mm/yr [Dewey et al., 1988; England and Molnar, 1998].

<sup>1</sup>Department of Earth and Space Sciences, University of California and Institute of Geophysics and Planetary Physics, Los Angeles, California, USA.

<sup>2</sup>Institute of Geophysics and Planetary Physics, Lawrence Livermore National Laboratory, Livermore, California, USA.

<sup>3</sup>Now at Department of Geosciences, University of Arizona, Tucson, Arizona, USA.

<sup>4</sup>Institute of Geology and Geophysics, Chinese Academy of Sciences, Beijing, People's Republic of China.

[3] In light of recent results of geologic and geophysical investigations in Tibet, these end-member views may require a level of refinement. Meyer *et al.* [1998], Owens and Zandt [1997], and Cattin and Avouac [2000] point out that discrete continental subduction may have been the dominant mode of deformation in accommodating the Indo-Asian collision along the northern and southern edges of the Tibetan plateau. This implies that extrusion tectonics may have played a lesser role in accommodating the overall convergence between India and Asia. This is consistent with the results of recent geologic and geodetic studies on major strike-slip faults in the Indo-Asian collision zone. For example, studies along the southern and central segment of the active right-slip Karakoram fault suggest that its total displacement is between 60 and 150 km, respectively [Searle, 1996; Searle *et al.*, 1998, 1999; Murphy *et al.*, 2000]. These estimates are much less than the  $\sim 1000$  km of right-slip motion predicted by the extrusion model [Peltzer and Tapponnier, 1988]. Using Quaternary slip rates along major strike-slip faults to test the extrusion hypothesis has yielded ambiguous results. At a timescale of a few years, GPS studies suggest that the Altyn Tagh fault moves at a rate of  $\sim 10$  mm/yr or less [Bendick *et al.*, 2000; Shen *et al.*, 2001]. However, long-term slip rates along the Altyn Tagh fault could be as high as  $\sim 30$  mm/yr [e.g., Meriaux *et al.*, 1999]. In addition, a recent study of the long-term slip rate along the Karakoram fault suggests that it may be as low as  $\sim 3$  mm/yr, based on dating offset geomorphic landforms using cosmogenic  $^{10}\text{Be}$  [Brown *et al.*, 2002]. Why slip rates along the Altyn Tagh and Karakoram faults vary with time remains poorly understood.

[4] Smaller magnitudes of displacement and slower slip rates along major strike-slip faults in Asia imply that eastward motion of Tibet may be less important than north-south shortening [England and Molnar, 1998]. However, this interpretation may be oversimplified, because eastward movement of Tibet could be accommodated by a greater number of strike-slip faults distributed over a large area of Tibet [Rothery and Drury, 1984; Molnar and Lyon-Caen, 1989; Yin, 2000]. If correct, then an alternative to the end-member models of discrete lateral extrusion and distributed crustal thickening arises. That is, eastward motion of Tibet could be accommodated by a large number of strike-slip faults distributed across central Tibet [Kong and Bird, 1996; Yin, 2000]. This interpretation implies that the left-slip Altyn Tagh and right-slip Karakoram faults may be only one of many conjugate fault systems that assist in the eastward spreading of the Tibetan crust (Foldout 1 and Figure 1). A key to testing this possibility is to establish the geometry and kinematics of active faults in the interior of the Tibetan plateau related to the Indo-Asian collision. Armijo *et al.* [1986, 1989] viewed the Qiangtang terrane as a rigid block moving eastward relative to the Lhasa terrane via a series of en-echelon right-slip faults (the Karakoram-Jiali fault zone) directly south of the Bangong-Nujiang suture zone. This interpretation has been questioned by both geophysical and geologic observations. First, active deformation is occurring in the Qiangtang terrane as expressed by numerous

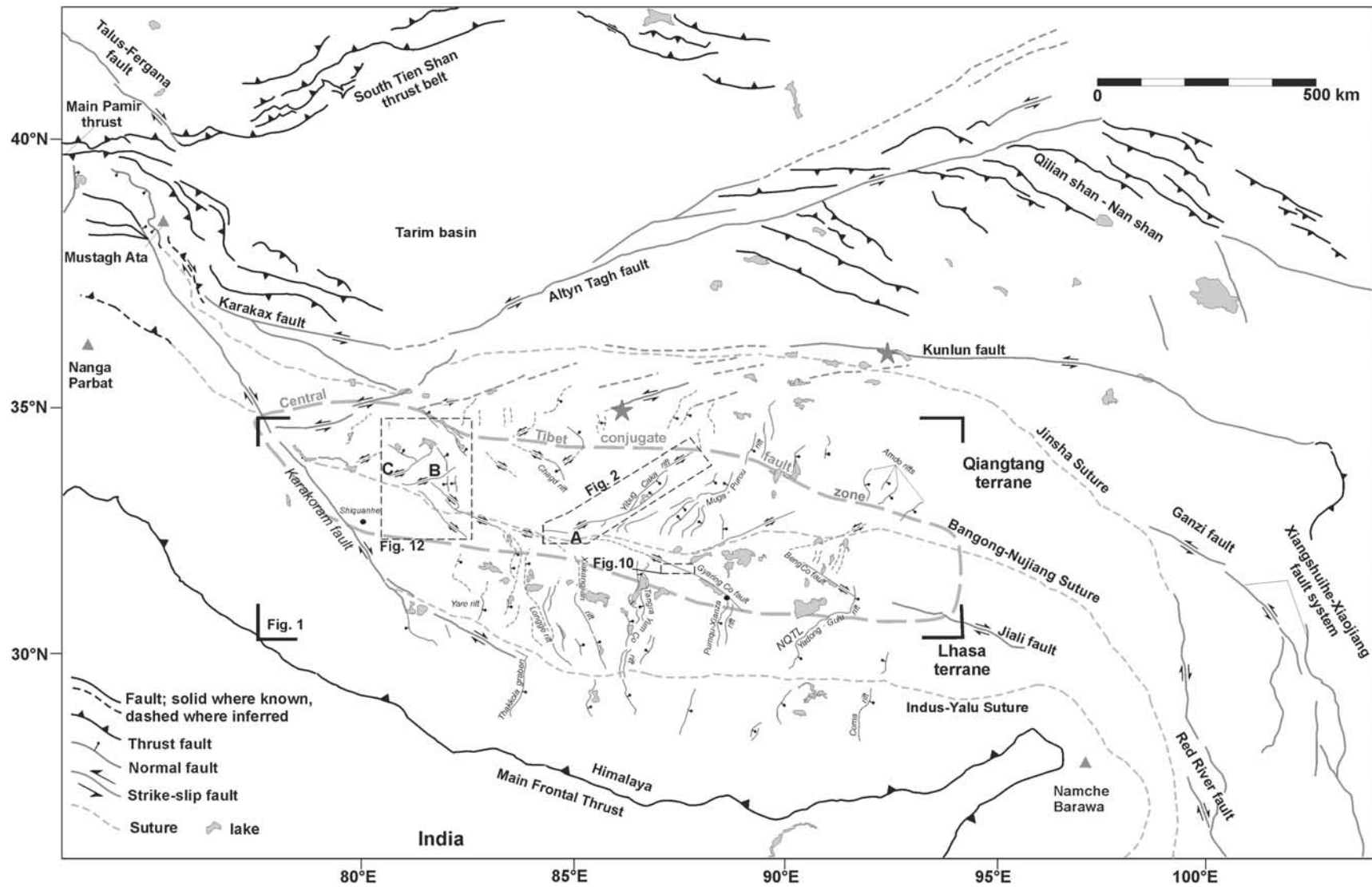
fault-bounded blocks with each having complex kinematics [Molnar and Lyon-Caen, 1989]. Second, field studies by Yin *et al.* [1999a] and Blisniuk *et al.* [2001] suggest that the Qiangtang terrane has experienced measurable east-west extension. In addition, a sparse GPS network that spans Tibet near  $95^\circ\text{E}$  longitude suggests that a measurable amount of coeval north-south contraction and east-west extension is presently occurring [Wang *et al.*, 2001].

[5] To address the question of how Tibet is deforming internally, we conducted geologic investigations of active-to-recently active faults using field mapping, analysis of digital topography (GTOPO30), and interpretation of Landsat-7 and CORONA satellite images. Our results allow us to develop a coherent kinematic model that emphasizes the role of conjugate strike-slip faults in accommodating coeval north-south contraction and east-west extension in central Tibet.

## 2. Regional Geology

[6] The Lhasa and Qiangtang terranes were accreted onto the southern margin of Eurasia beginning in the north, during the Late Triassic-Early Jurassic and the Late Jurassic-Early Cretaceous [Dewey *et al.*, 1988; Yin and Harrison, 2000]. From north to south, the boundaries of these terranes are marked by the Jinsha, Bangong-Nujiang, and Indus-Yalu suture zones and have been reactivated by both strike-slip and contractional deformation during the Cenozoic Indo-Asian collision [Armijo *et al.*, 1986, 1989; Meyer *et al.*, 1998].

[7] A salient topographic feature of the Lhasa terrane is the north trending rift systems, which dissect the otherwise low-relief surface. Whether the rifts are an expression of upper crustal deformation or involve the mantle lithosphere has been debated [Masek *et al.*, 1994; Yin, 2000]. It has also been considered that Tibetan rifts are the result of gravitational collapse [Molnar and Tapponnier, 1978; Tapponnier *et al.*, 1981] or caused by a convective event in the mantle [England and Houseman, 1989]. Except the Yadong-Gulu rift that extends into the Himalaya, all rifts in the Lhasa terrane terminate before they reach the Indus-Yalu and Bangong-Nujiang suture zones [Armijo *et al.*, 1986]. This observation implies that the sutures on both sides of the Lhasa terrane may act as transfer structures converting east-west extensional strain to the Qiangtang terrane in the north and southward into the Himalayan range [Yin, 2000]. The initiation of the Yadong-Gulu rift is constrained to be  $8 \pm 1$  Ma along the Nyainqentanghla Shan [Harrison *et al.*, 1995], with an upper age bound of  $\sim 12$  Ma along its southernmost segment [Edwards and Harrison, 1997; Wu *et al.*, 1998]. Minor east-west stretching of the Lhasa crust at an earlier stage is inferred from a north trending dike swarm near Xigaze and was dated at 18–13 Ma [Yin *et al.*, 1994; Williams *et al.*, 2001]. The Thakkola graben in the central Himalaya south of the Lhasa terrane initiated between 11–14 Ma based on ages of the oldest synrift sediments [Garizone *et al.*, 2000] and north trending extensional fractures [Coleman and Hodges, 1995].



**Foldout 1.** Regional tectonic map of the Tibetan plateau modified after *Armijo et al.* [1986, 1989], *Meyer et al.* [1998], *Arrowsmith and Strecker* [1999], *Yin et al.* [1999b], and our own observations. Inactive structures (e.g., the Gandese thrust) in central Tibet have been omitted for clarity. An east-west trending belt of conjugate strike-slip faults is present along the Bangong-Nujiang suture zone in central Tibet. See text for description of the fault geometry and distribution of sutures. Red stars indicate the locations of the 8 November 1997, M7.6 left-slip Manyi earthquake (left), and the 14 November 2001, M7.9 left-slip Kokoxilli earthquake (right). Labels A, B, and C indicate the intersections of the Dong Co, Bue Co, and Aishi Co conjugate strike-slip fault systems. See enlarged version of this figure in the HTML.

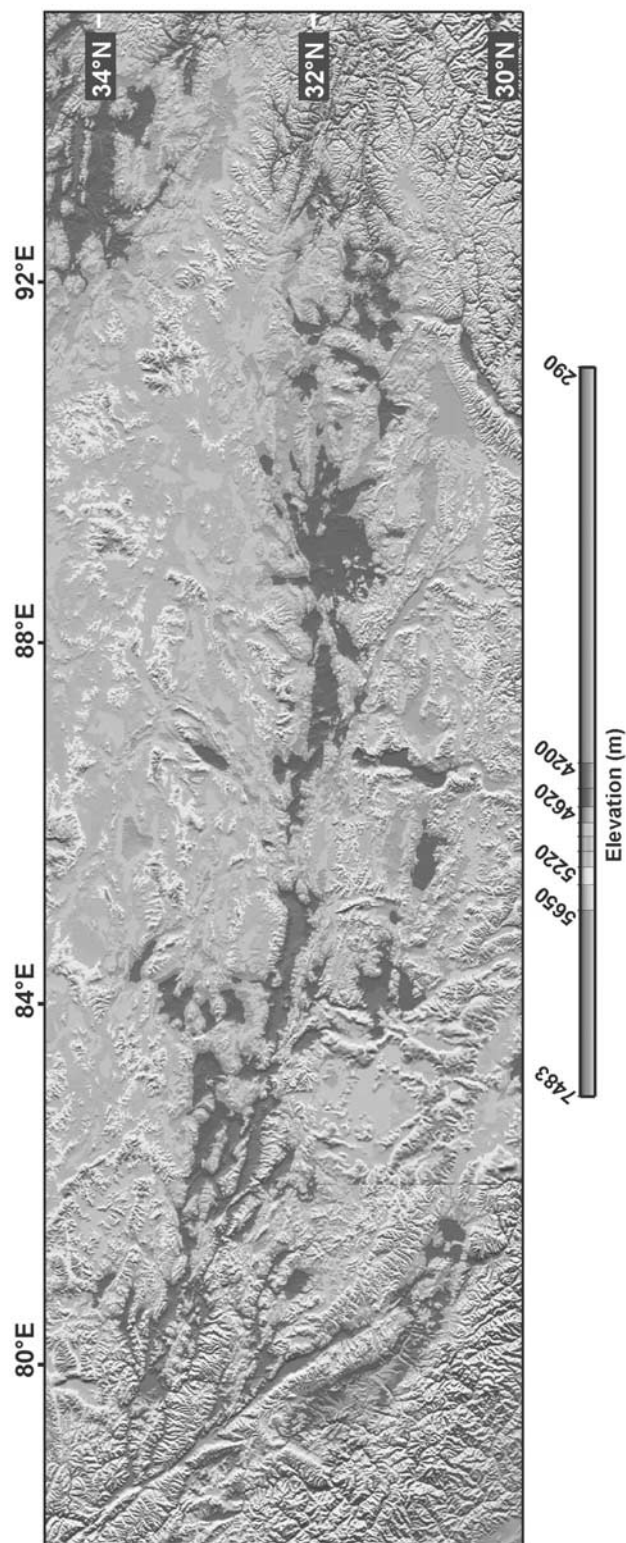


**Figure 1.** Color shaded relief map with a compressed palette of central Tibet showing a broad east-west trending depression (in dark blue) along the Bangong-Nujiang suture zone. Note that the depression is marked by a series of discontinuous basins. Strike-slip faults are represented by narrow and linear topographic structures trending northeast and northwest, north and south of the central depression. These linear features are the left-slip faults in the Qiangtang terrane and right-slip faults in the Lhasa terrane. Note that right-slip faults in the Lhasa terrane bound the northern margin of several north trending rifts, whereas left-slip faults in the Qiangtang terrane are connected with topographically less pronounced north trending rifts. The poor topographic definition of rifts in Qiangtang may result from the internally drained basin filling [Yin *et al.*, 1999b], or because of horizontal motion associated with strike-slip faulting. See color version of this figure at back of this issue.

[8] Active faulting within the Qiangtang terrane has been recognized previously through fault plane solutions and analysis of satellite imagery [Molnar and Lyon-Caen, 1989; Molnar and Tapponnier, 1978; Rothery and Drury, 1984]. These studies revealed that active-to-recently active faults in the Qiangtang vary in strike and fault kinematics. The latter ranges from strike-slip to normal faulting. A minimum initiation age of normal faulting was obtained by Blisniuk *et al.* [2001], who used the  $^{40}\text{Ar}/^{39}\text{Ar}$  method to date syn-kinematically grown muscovite from the Shuanghu normal fault zone. Their results suggest that the onset of east-west extension may have occurred at or prior to  $\sim 13.5$  Ma [Blisniuk *et al.*, 2001]. Similar to rifts in the Lhasa terrane, rifts and their associated faults in the Qiangtang terrane do not appear to extend across the Bangong-Nujiang suture zone, suggesting that it has been acting as a transfer zone linking extensional structures in the Lhasa and Qiangtang terranes [Yin, 2000]. It is the question of how the extensional structures are geometrically and kinematically related across the Bangong-Nujiang suture zone that has motivated this study as presented in detail below.

### 3. Conjugate Faults Along the Bangong-Nujiang Suture Zone

[9] From field observations, topography, and satellite images, faults that appear to be active and located directly north of the Bangong-Nujiang suture zone are exclusively northeast striking while those directly south of the suture are northwest striking [Rothery and Drury, 1984; Armijo *et al.*, 1986]. These faults merge toward one another along the suture (Foldout 1 and Figure 1). Because north trending rifts in Lhasa and Qiangtang accommodate nearly east-west extension [Mercier *et al.*, 1987; Yin *et al.*, 1999a], an inference is that northeast striking faults are left-slip, whereas the northwest striking faults are right-slip. This would imply that these structures are conjugate fault sets that accommodate coeval east-west extension and north-south contraction. In the following, we show that conjugate strike-slip fault systems are common structures in central Tibet, which all together accommodate a portion of Indo-Asian convergence.

#### 3.1. Dong Co Conjugate System

[10] The east facing Dong Co conjugate fault system is comprised of the northeast striking Yibug Caka fault zone to the north and the northwest striking Gyaring Co fault to the south (Foldout 1 and Figure 1). We have mapped the bedrock geology of the conjugate fault system on 1:100,000 scale topographic maps. In the vicinity of active-to-recently active faults, we mapped the Quaternary stratigraphy on CORONA satellite photographs. Quaternary units were delineated based on their relative surface heights and roughness, degree of surface vegetation and incision, and surface albedo observed in satellite images and in the field.

##### 3.1.1. Left-Slip Yibug Caka Fault Zone

[11] The  $\sim 340$  km long Yibug Caka fault zone is S-shaped in map view, with the northern and southern segments

striking  $\sim \text{N}70^\circ\text{E}$  and the central segment striking  $\text{N}30\text{--}40^\circ\text{E}$  (Foldout 1 and Figures 1 and 2). The northern and southern fault segments are dominantly left-slip, whereas the central fault segment is dominantly normal-slip (Figures 2b–2d). Associated with along-strike variation of fault strike and kinematics is a change in topographic relief. Local relief is  $\sim 500$  m along the strike-slip segments of the fault zone, but increases to  $>1000$  m along the normal-fault segment (Figure 2a).

[12] The Riganpei Co fault defines the southern Yibug-Caka fault zone and strikes  $\text{N}70^\circ\text{E}$ . Locally, it exhibits sub-horizontal fault striations (Figure 2). The fault offsets left-laterally a north dipping thrust at its northeast end for  $\sim 7$  km (Figure 2a). The thrust juxtaposes Permian limestones over folded Tertiary strata. The Riganpei Co fault locally offsets alluvial fans and paleo-shorelines, as observed near Riganpei Co (Figure 6). The Riganpei Co fault becomes buried, or tips out at its southern end at the Zhaxi Co and Dong Co basins (Figure 2a). Although northeast striking fault scarps are locally observed near Zhaxi Co, these faults disappear to the south. The northern end of the Riganpei Co fault links with an extensional system in the central Yibug-Caka fault zone.

[13] Locally, pressure ridges, sag ponds, and offset alluvial fans are observed along the Riganpei Co fault (Figure 3). Field observations allow us to identify four chronostratigraphic units (Qa1–Qa4 from oldest to youngest, Figure 3). The right stepping, en echelon alignment of the fault traces and ridges is consistent with left-slip motion. South flowing streams are also offset left laterally (Figure 4). Field measurements of the offset gullies and beheaded channels range from 30–100 m. The variations in horizontal displacement presumably reflects the relative ages of the offset geomorphic features with the least incised and smoothest (i.e., youngest) and relatively lower alluvial surfaces displaying the smallest offsets. Locally, shutter ridges are present along the active trace of the Riganpei Co fault with an average trend of  $\text{N}70^\circ\text{E}$ . Shutter ridges are typically several hundred meters in length and tens of meters in height. They are asymmetric in cross-section, where the north sides of the shutter ridges are steep and coincident with the sub-vertical fault surface (Figure 4).

[14] In the vicinity of Riganpei Co, regressive shorelines are observed with overlying younger alluvial sediments. In turn, the alluvial sediments are cut by several anastomosing strands of the Riganpei Co fault (Figure 5). Left-lateral offset of the alluvial fans is observed on their eastern margin where a north facing fault scarp indicates left-lateral and dip-slip displacements of  $25 \pm 5$  m and  $2 \pm 0.5$  m, respectively, as determined in the field with a tape measure and Brunton clinometer (Figure 5). A left-lateral offset of a channel is also  $25 \pm 5$  m at this site (Figure 5a). Most lakes and closed basins in Tibet are surrounded by regressive shorelines. An example from west central Tibet is Longmu Co, where the shorelines were leveled from 75–250 m above the present lake level [Avouac *et al.*, 1996]. A modified Penman formula was used to calculate a synthetic curve of the shoreline regression at Longmu Co [Avouac *et*

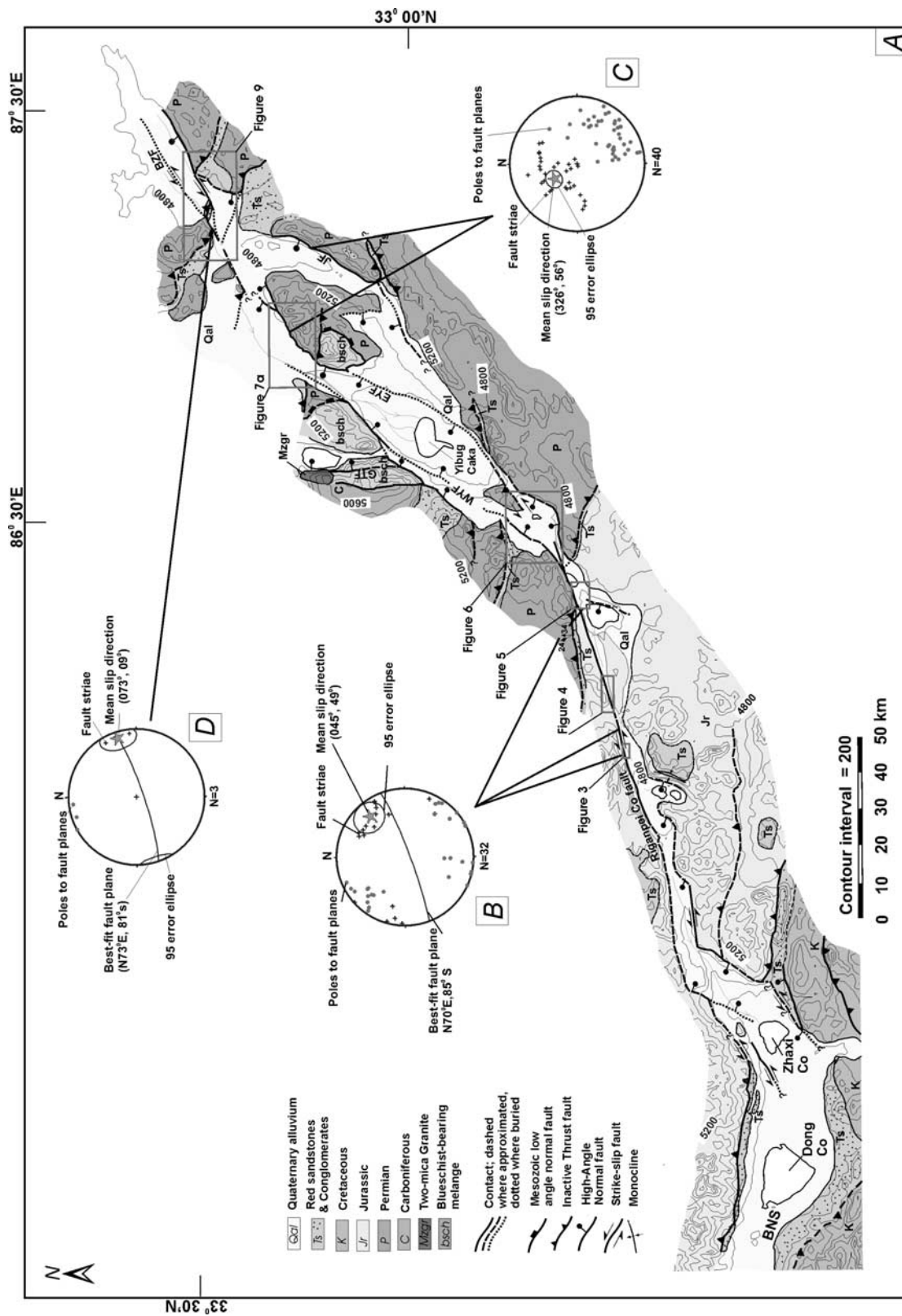
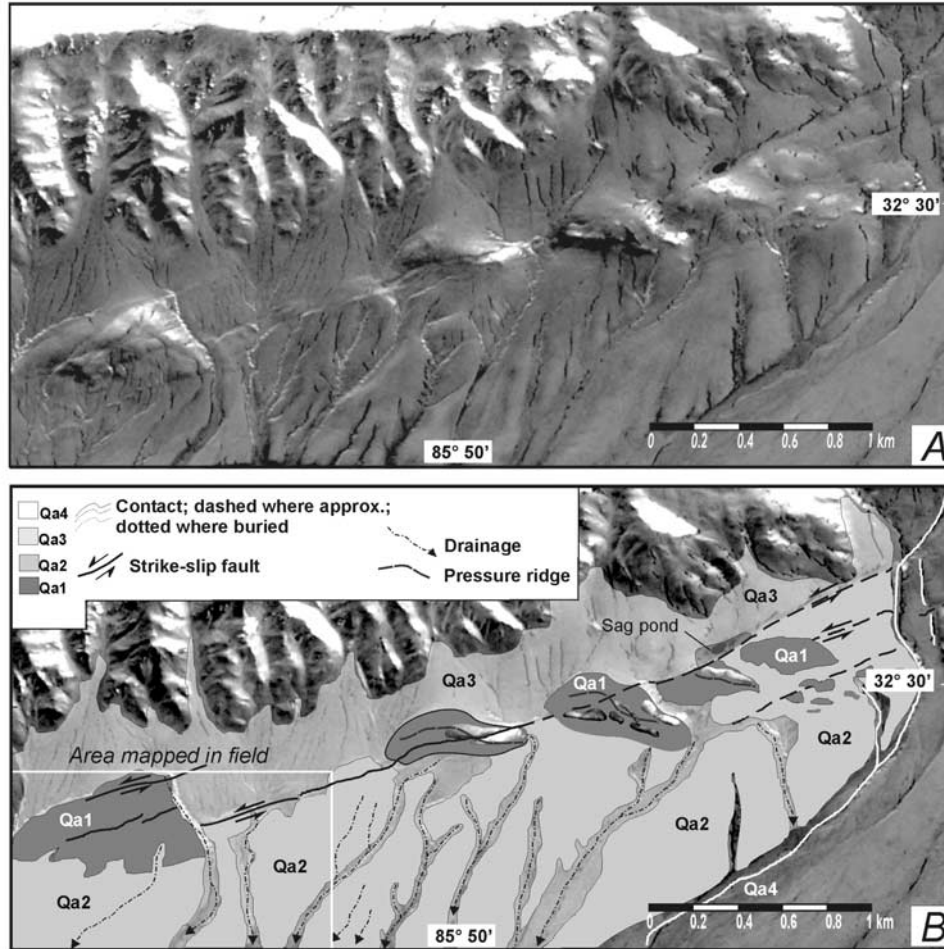


Figure 2. (a) Simplified tectonic map of the Yibug Caka fault zone, Qiangtang. (b), (c), and (d) are lower hemisphere stereographic projections of fault kinematic data. GTF = Gangtang fault, WYF = West Yibug Caka fault, EYC = East Yibug Caka fault, JF = Jiamou fault, BZF = Bu Zang Ai fault. See color version of this figure at back of this issue.



**Figure 3.** Relationships between tectonic landforms, Quaternary units, and the Riganpei Co fault. (a) CORONA satellite image of the fault trace associated with transpressional structures. The en echelon alignment of the ridges and the right-stepping fault traces indicates a local strain field consistent with left-slip motion. (b) Quaternary geologic map based on field observations made in the southwestern part of the map area and interpretation of CORONA imagery in (a). The map shows locations of fault strands, offset drainages, a sag pond, and obliquely oriented pressure ridges with respect to the fault trace. Note that a pressure ridge is observed where the left-slip fault steps right. See text for details on criteria used for separating mapped units. See Figure 2a for location.

*al.*, 1996]. It was determined that a rapid shoreline regression dropped the lake level by about 160 m, which occurred for a duration of 120 years after the lakes reached their highest stand at  $\sim 7.6$  ka [Avouac *et al.*, 1996]. Although the exact cause for the shoreline regression is unknown, it may be a result of a regional climatic effect [Avouac *et al.*, 1996].

[15] The Riganpei Co fault terminates into the extensional Riganpei Co basin (Figures 2a and 6). Faulting is observed along the western margin of the basin and is expressed by several southeast and northeast facing scarps cutting alluvial fans (Figure 6). Three topographic profiles were surveyed across the southeast facing scarps using a tape measure and Brunton clinometer, which indicate a 7.5 m vertical offset (Figure 6). The profiles consist of 67 (profile 1), 76 (profile 2), and 97 (profile 3) measured

points, with an uncertainty derived from reading the slope angle, which is  $\pm 1^\circ$ .

[16] The central Yibug-Caka fault zone trends  $\sim N30-40^\circ E$  and is characterized by several fault-bounded tilted blocks and interlying NNE trending basins in between (Figure 2a). The range-bounding faults include the Gangtang Co, West Yibug Caka, East Yibug Caka, and Jiaomu faults, which strike NNE and cut both bedrock and alluvial sediments (Figure 7). The West Yibug Caka fault is east dipping and is geometrically linked to the Riganpei Co fault (Figure 2a). To the north, the West Yibug Caka fault becomes antithetic to the East Yibug Caka fault and transfers WNW-ESE extension to two west dipping normal faults: the East Yibug Caka and Jiaomu faults. To the north, the north striking faults merge with Bu Zhang Ai left-slip fault in the northern segment of the Yibug-Caka fault zone.

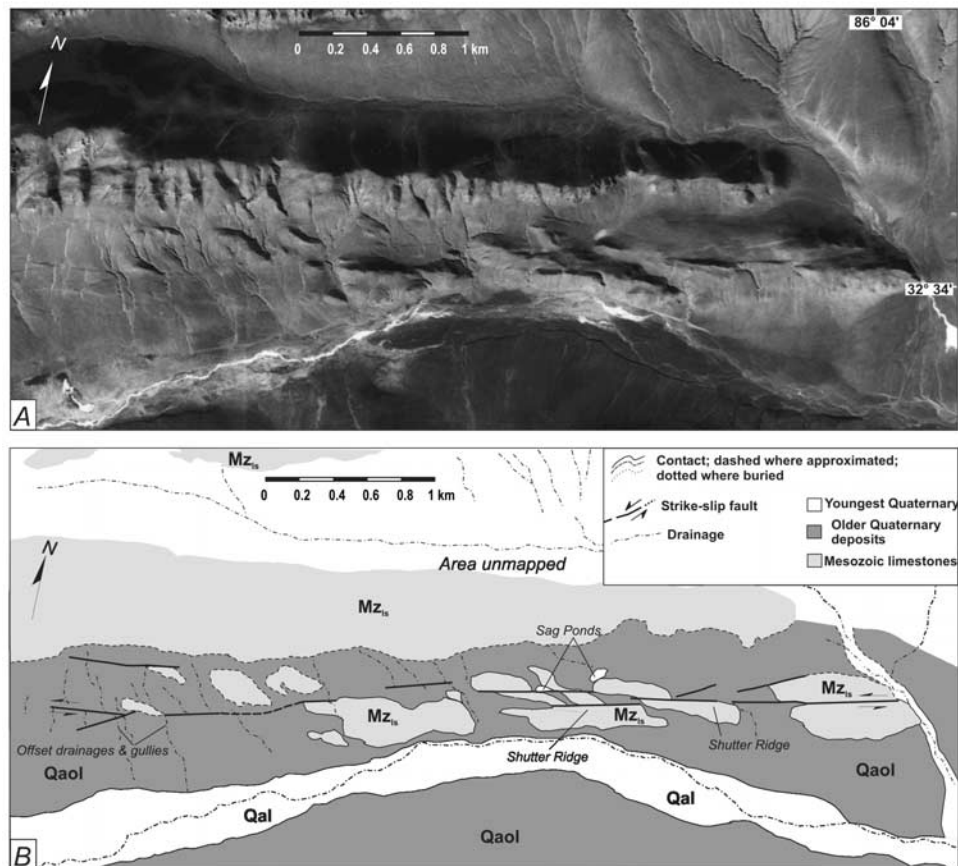


**Figure 4.** (a) CORONA satellite imagery of neotectonic features along a potentially active fault zone. Landforms include offsets of drainages, shutter ridges, and sag ponds that are consistent with left-slip motion. (b) Line drawing of the major geologic features observed in the field and shown in (a). See Figure 2a for location.

[17] The NNE striking faults in the central fault zone are normal-slip as indicated by dip-slip fault striations (Figure 2c), toolmarks, mullions, and Riedel shears (Figure 8a). The striation data were collected only from the range-bounding faults, as minor faults located away from the main fault zone may be unrelated to the Yibug Caka fault. The best fit mean slip direction for west dipping faults is  $326^{\circ}$ ,  $56^{\circ}$  (Figure 2c).

[18] The central block in the northern half of the central Yibug Caka fault zone exposes blueschist-bearing melange. Its exhumation is associated with motion along the early Jurassic Rongma detachment fault, which is related to a regional early Mesozoic extensional event that occurred throughout the central Qiangtang [Kapp *et al.*, 2003; Kapp, 2001]. The Rongma detachment fault is regionally extensive and forms a key marker horizon for restoring the magnitude of extension across the active normal faults in the central Yibug Caka fault zone. Although the uncertainties are large, a minimum of 2 km of east-west extension is accommodated by the NNE striking faults that are distributed across the central Yibug Caka fault zone [see Kapp *et al.*, 2003].

[19] The Bu Zang Ai fault segment of the Yibug Caka fault zone strikes  $N73^{\circ}E$  and is dominantly left-slip.

Locally, sub horizontal striations and tool marks are observed on fault surfaces and indicate a mean slip direction oriented  $073^{\circ}$ ,  $09^{\circ}$  (Figure 2d). We estimate the magnitude of left slip along this fault segment to be  $\sim 14$  km based on the left-separation of a north dipping Tertiary thrust. The thrust juxtaposing Paleozoic limestones over Tertiary red beds is truncated by two strands of the strike-slip system that strike  $\sim N55^{\circ}E$  (Figures 2a and 9). The thrust is oroclinally folded as it approaches the fault zone from a moderate dip of  $47^{\circ}$  in the east, and becomes subvertical in the west (Figure 9). We suggest that synkinematic transform motion related to thrusting in the Quaternary is unlikely, as no thrust fault scarps are observed, and locally Quaternary sediments unconformably overlie the thrust contact.

[20] Although we only visited the southernmost part of the northern rift segment, the morphologically defined Yibug Caka rift extends for at least another 50 km to the north (Figure 2a). From topography and existing active tectonic maps of the region [Liao, 1990], it appears that the Yibug Caka rift transfers displacement to a series of north trending rifts in the north. These rifts in turn, appear to terminate into a series of ENE striking left-slip faults that we consider as the westernmost extension of the seismically

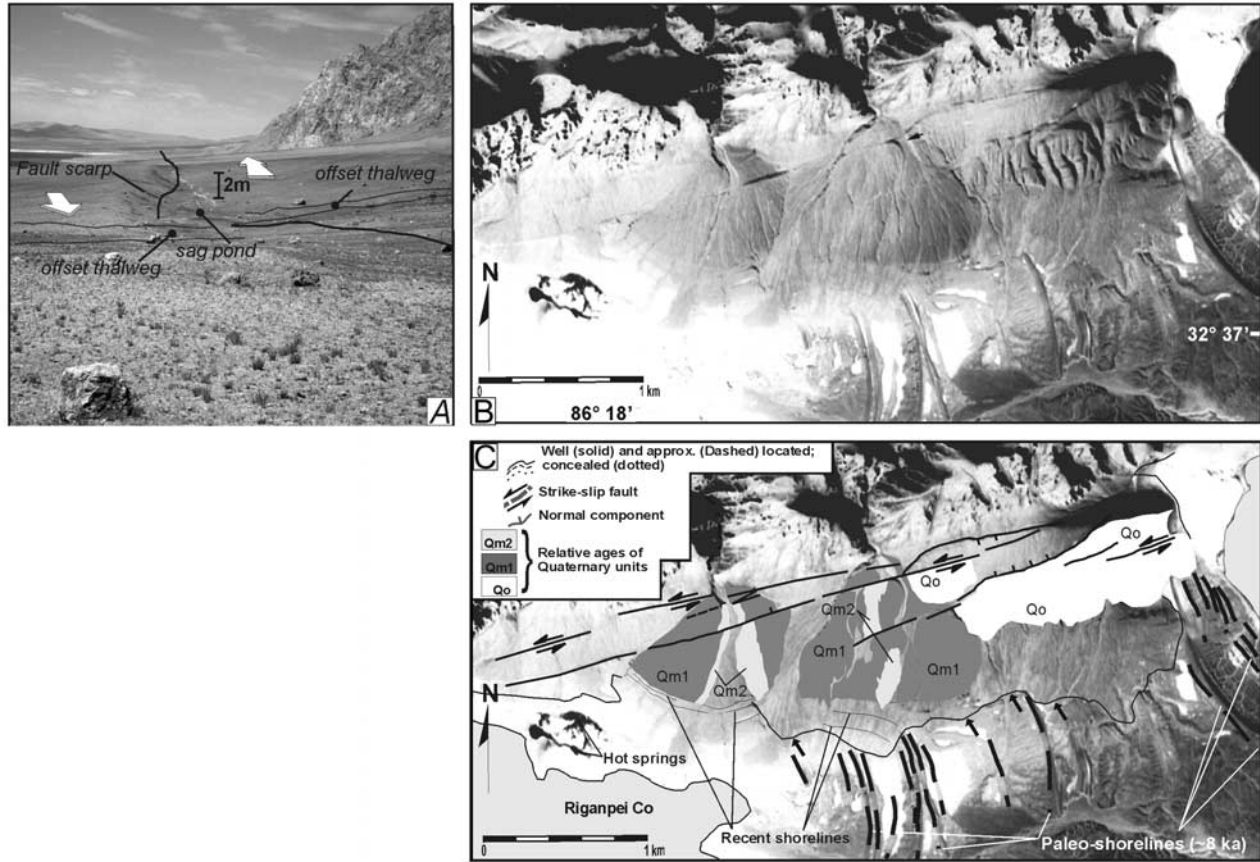


**Figure 5.** (a) Field photo looking WSW along a fault scarp that cuts alluvial fans along the northern segment of the Riganpei Co fault. The fault scarp is north facing and offsets a drainage for  $\sim 30$  m left laterally. (b) CORONA imagery of the fault trace. (c) Line drawing of geologic relationships based on field mapping and interpretation of (b). Note that younger alluvial deposits, which are cut by the fault strands, depositionally overlie the regressive shorelines as shown by the green arrows. See Figure 2a for location.

active left-slip Kunlun fault system [Kidd and Molnar, 1988; Yin, 2000; Van der Woerd *et al.*, 2000, 2002]. This inference is consistent with the left-slip focal mechanisms of the M 7.6 and M 7.9 Manyi and Kokoxilli earthquakes, which occurred along the inferred left-slip faults (Foldout 1 and Figure 1) [Peltzer *et al.*, 1998; Lasserre *et al.*, 2002].

### 3.1.2. Right-Slip Gyaring Co Fault

[21] From regional mapping, topographic maps, and Landsat images, the left-slip Riganpei Co fault in the southern Yibug Caka fault zone merges to the south with the right-slip Gyaring Co fault in the northern Lhasa terrane (Foldout 1 and Figure 1). This relationship suggests that the two faults may form a conjugate strike-slip set, which would require a comparable magnitude of displacement across the two faults. Right-slip faults directly south of the Bangong-Nujiang suture, namely the Karakorum-Jiali fault zone [Armijo *et al.*, 1986, 1989], are kinematically related to north trending rifts further to the south [Mercier *et al.*, 1987; Burchfiel *et al.*, 1991; Ratschbacher *et al.*, 1994; Harrison *et al.*, 1995; Cogan *et al.*, 1998]. Four of these strike-slip faults, the Karakorum fault, the Gyaring Co fault,

the Jiali fault, and the Beng Co fault were studied by Armijo *et al.* [1989]. However, that study emphasized the neotectonic activity of these structures and provides no constraints on the magnitude of fault slip. Thus, our study, with an emphasis on determining piercing points across the right-slip faults in the northern Lhasa terrane compliments the work of Armijo *et al.* [1989]. The results of our investigation on the Gyaring Co fault are described below.

[22] The Gyaring Co fault is expressed as a linear valley  $\sim 250$  km long that strikes  $\sim N70^\circ W$ . Its northern end merges with the southern end of the Yibug Caka fault zone along the Bangong-Nujiang suture, whereas its southern end is kinematically linked with the north trending Pum-Qu-Xainza rift (Foldout 1 and Figure 1). Our fieldwork concentrated on the northern fault segment where the fault offsets Mesozoic and Early Tertiary east trending contractional structures and strata (Figure 10a). The fault is sub-vertical and well exposed along the northwest shore of Goman Co. Striations in the fault zone are dominantly horizontal and the fault zone gouge can reach tens of meters in thickness. Locally, the trace of the fault cuts alluvial

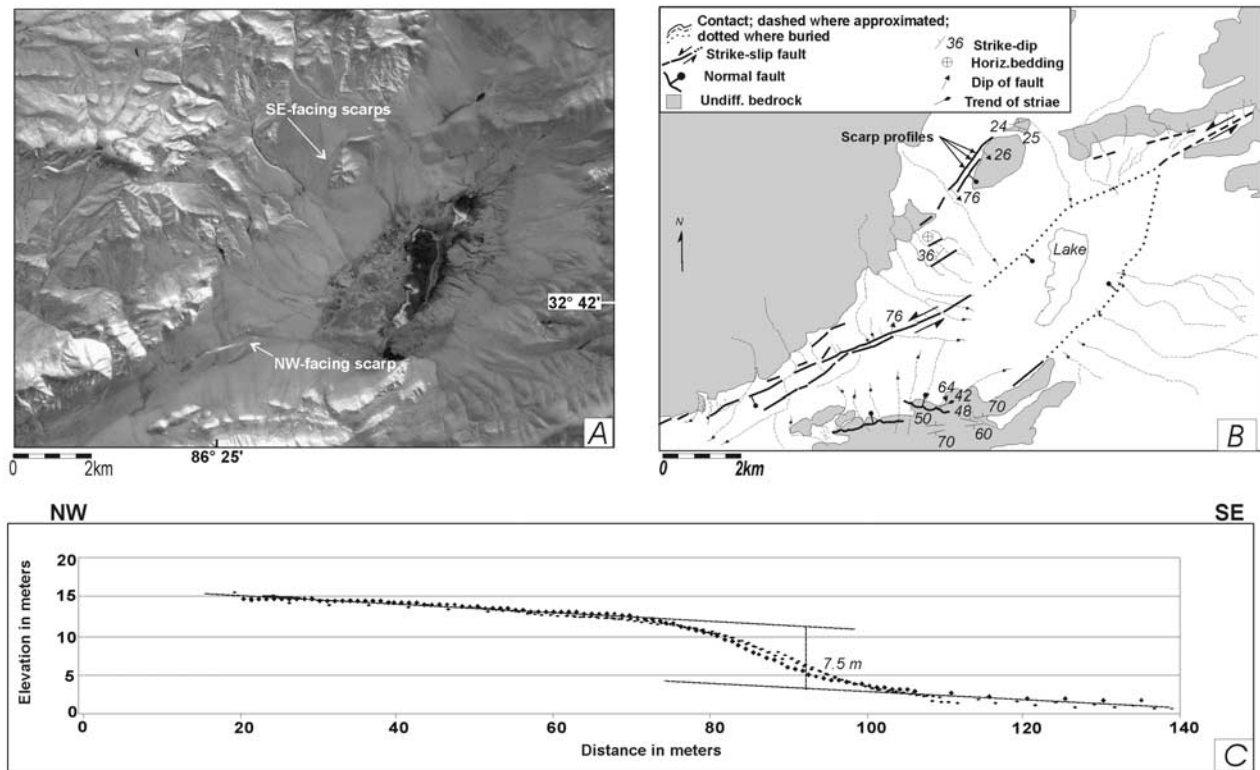


**Figure 6.** (a) CORONA imagery of the Riganpei Co basin at the northern end of the Riganpei Co fault. (b) Line drawing of key geologic relationships as observed in the field and interpreted from (a). Both normal and strike-slip faults cut Quaternary alluvial deposits in the transtensional structure. (c) Fault scarp profiles surveyed with tape measure and Brunton clinometer. See (b) for location of scarp profiles and Figure 2a for location.

sediments and is associated with sag ponds, pressure ridges, offset alluvial fans and terrace risers, all consistent with right-slip motion.

[23] The magnitude of slip on the Gyaring Co fault is constrained by restoring a piercing point defined by the intersection line between a Tertiary unconformity (defined by Tertiary strata deposited on top of Mesozoic strata) and the Goman-Caibu Co thrust system, both of which are cut by the strike-slip fault (Figures 10 and 11). The Goman-Caibu Co thrust system juxtaposes Early Cretaceous limestones over younger Cretaceous volcanic rocks, and Tertiary sandstones and conglomerates, all offset by the Gyaring Co fault. The age assignment of stratigraphic units observed in the study area is adopted from Liu [1988]. Because the Goman-Caibu Co thrust system cuts Tertiary strata, the offset of this structure by the Gyaring Co fault can be attributed to its Late Cenozoic motion. A best fit plane to the Goman-Caibu Co thrust is oriented  $N75^{\circ}E, 24^{\circ}NW$  (Figure 10d). Measurements of the footwall stratigraphic bedding and the underlying unconformity indicate a best fit plane oriented  $N81^{\circ}E, 14^{\circ}NW$  (Figure 10c). The trend and plunge of the intersection line between the two best fit planes is  $257^{\circ}, 01^{\circ}$  (Figure 10b). The offset calculation of this intersection line uses a best fit orientation of the Gyaring Co fault. Fault zone fabrics are well exposed along

the north shore of Goman Co. Measurements of fault surfaces indicate a best fit fault plane oriented  $N70^{\circ}W, 89^{\circ}NE$  (Figure 10d). We project the intersection line between the Goman-Caibu Co thrust systems and the Tertiary unconformity into the plane of the Gyaring Co fault. The intersection line pierces the Gyaring Co fault in the west and east sides at the 4710-m and the 4610-m structure contours, respectively. A calculated net slip is  $12.5 \pm 4$  km oriented  $110^{\circ}, 5^{\circ}$ . A minor normal component of  $\sim 100$  m is calculated from the total slip vector. The uncertainty in the slip calculation is introduced due to uncertainties in the location of the intersection line, which result from errors associated with the fault orientation and the attitude of the Tertiary unconformity.

[24] A similar magnitude of right separation along the Gyaring Co fault may be inferred to the northwest, based on the  $\sim 12$  km of right separation of a north dipping thrust juxtaposing Mesozoic carbonates over Mesozoic volcanic rocks (Figure 10). The initiation age of the Gyaring Co fault is unknown.

### 3.2. Bue Co Conjugate System

[25] The Bue Co conjugate fault system is located  $\sim 400$  km west of the Dong Co conjugate system and consists of two fault segments that conjoin at Bue Co

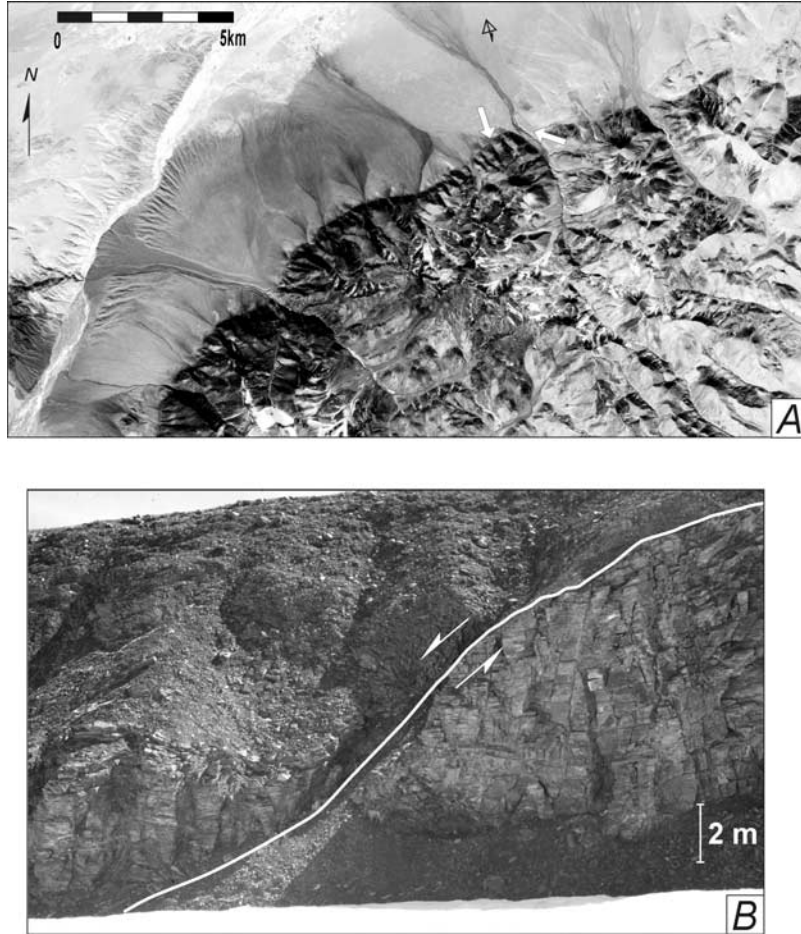


**Figure 7.** (a) CORONA imagery showing western margin of a range front bounded by a west dipping normal fault. Northwest trending, white arrow indicates location of normal fault in Figure 7b. Southeast trending, white arrow at the range front indicates location of Figure 8a; symbol on alluvial fan indicates viewing location and viewing direction for Figure 8b. (b) A west dipping normal fault offsetting the contact between Quaternary fan deposits above and the Paleozoic strata below, view is to the north. See (a) for location.

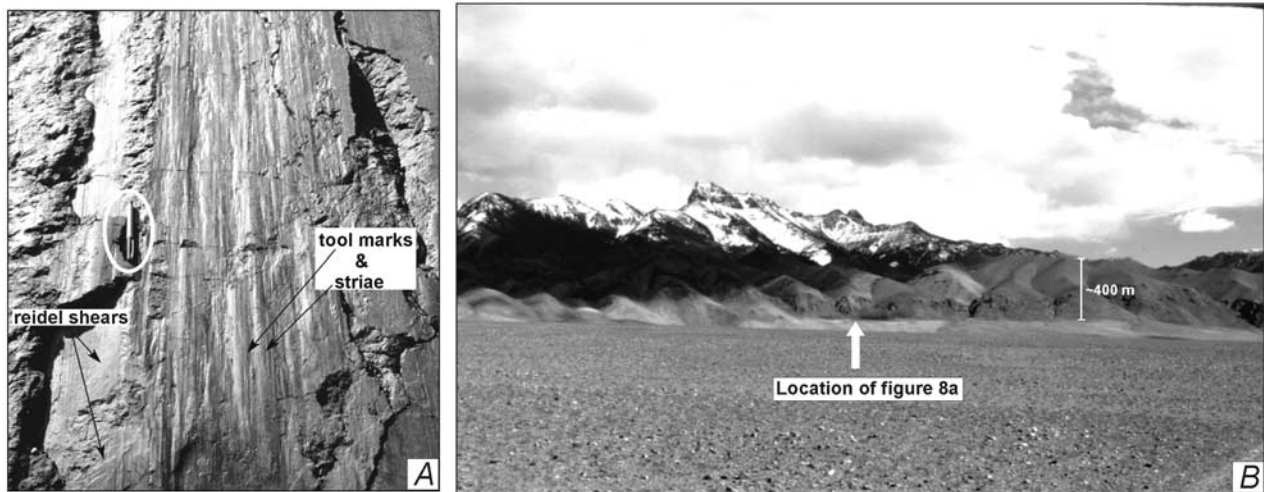


**Figure 8.** (a) Downdip fault striations, toolmarks and reidel shears on surface of a west dipping normal fault, view to the east. Location of this outcrop is indicated in Figure 7a by southeast trending white arrow. (b) West dipping normal fault, view to the ESE. See Figure 7a for location.

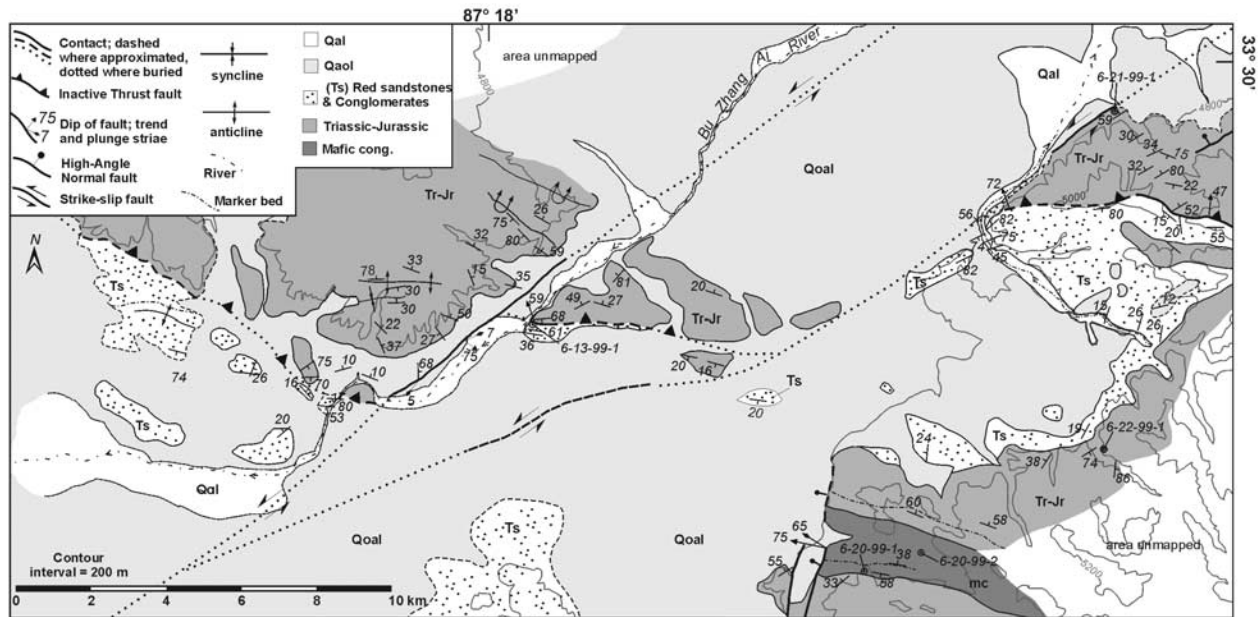


**Figure 9.** Geologic map of the Bu Zhang Ai fault zone. Strike-slip faults cut a north dipping thrust along the northern rift segment of the Yibug Caka rift. See Figure 2a for location.

(Figure 11). The Bue Co fault strikes  $N70^{\circ}E$  and forms the northern branch of the strike-slip conjugate system and the Lamu Co fault strikes  $N55^{\circ}W$  and forms the southern branch. The Bue Co fault forms a broad valley up to 10 km wide and  $\sim 80$  km long. Along strike to the northeast, the fault merges with two northeast dipping faults that bound the elongate basins (Figure 12). The main Bue Co fault displays an apparent left-oblique normal-slip component (Figure 14). This interpretation is based on the presence of a  $\sim 25$  km long and  $\sim 7$  km wide crescent-shaped basin that is bounded on its east side by the southern Bue Co fault. We interpret this basin geometry to result from left-slip motion along a releasing bend (Figure 12). The active nature of the fault is suggested by its trace cutting several alluvial fans (Figure 13a). The magnitude of left-lateral motion along the Bue Co fault is  $\sim 12$  km, as estimated from left separation of a Permian limestone unit [Cheng and Xu, 1987] observed in Landsat-7 imagery (Figure 13).

[26] The Lamu Co fault strikes  $\sim N55^{\circ}W$  and consists of two segments (Figure 13). The overlapping area of the two right stepping fault segments resembles a pull-apart basin. If correct, this implies that the Lamu Co fault is right-slip. The northern fault segment strikes  $N50^{\circ}W$  and is  $\sim 45$  km long. Fault scarps and triangular facets are visible in Landsat images, suggesting that this structure may be active (Figure 13a). Jurassic volcanic strata [Cheng and Xu, 1987] at location A-A' are truncated by the fault and display  $\sim 11$  km of right separation (Figure 14). The southern fault segment of the Lamu Co fault is also visible on Landsat-7 images (Figure 13a). It is curvilinear in map view, is  $>95$  km long, and truncates east-west striking Jurassic strata.

[27] Distinct Jurassic volcanic rocks appear as a dark red lithologic unit in the center of Figure 13a. This unit

coincides with a south-directed thrust fault that was mapped on the western side of the Lamu Co fault [Cheng and Xu, 1987]. This contact is truncated by the Lamu Co fault at location B in Figure 13b. A red lithologic unit with similar characteristics and geometry is observed on the eastern side of the Lamu Co fault as recognized from the Landsat-7 image (B' on Figure 13b). Because the two units appear similar, we suggest that they were once the same unit that has been cut by the Lamu Co fault. This implies  $17 \pm 5$  km of right separation along the Lamu Co fault.

[28] The triangular block bounded by the conjugate Bue Co and Lamu Co faults appears to be undergoing east-west extension. This inference is suggested by the presence of three north trending range fronts with triangular facets bounding their western margins (Figure 13a). Although the data are sparse, we interpret this range front morphology to represent active-to-recently active faulting (Figure 13a). Based on the locations of the adjacent basins with respect to the north-south strike of the range-bounding features, we infer these to represent west dipping extensional structures. A basin is located at the tip of the wedge-shaped block bounded by the Bue Co and Lamu Co faults. This basin appears to be transtensional [Harland, 1971] in origin because of the eastward extrusion of the small wedge-shaped block that leaves a space at its trailing end. A prediction of this model is that the kinematics of range-bounding faults would have a dominant component of oblique strike-slip motion.

### 3.3. Aishui Co Conjugate System

[29] The Aishui Co conjugate fault system is located  $\sim 70$  km west of the Bue Co conjugate fault system. This fault system consists of the left-slip Xianqie Co fault in the north and the right-slip Awong Co fault in the south. Investigation of this conjugate fault system is based on



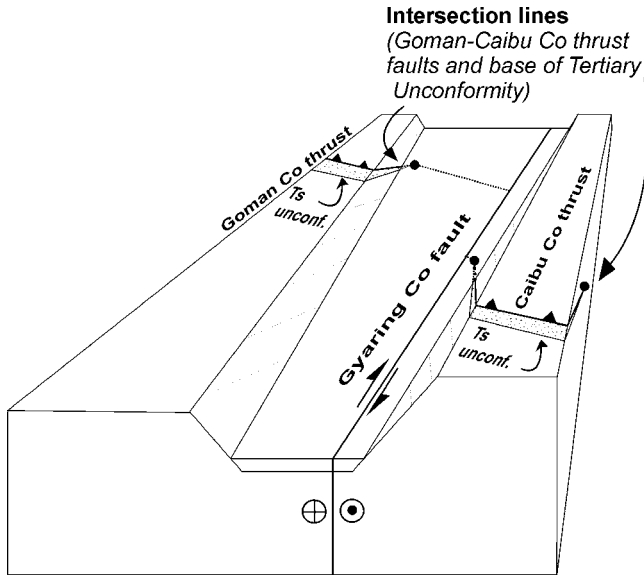


**Figure 11.** A simple block diagram illustrating the offset relationships of the Goman-Caibu Co thrust systems along a simplified trace of the Gyaring Co fault.

digital topography, satellite images, and reinterpretation of existing geologic maps [Liu, 1988; Cheng and Xu, 1987].

### 3.3.1. Left-Slip Xianqie Co Fault System

[30] The Xianqie Co fault is comprised of two principal fault segments that strike  $N65^{\circ}E$  and are defined by the presence of three lakes (Figure 12). The southern segment of the Xianqie Co fault system begins at the Quaternary Aishui Co basin in the south and links with the northern fault segment at Xianqie Co. The northern fault segment continues from Xianqie Co in the south and appears to terminate at Lumajangdong Co in the north (Figure 12). The Aishui Co basin may be associated with an east trending contractional structure whereas the Xianqie Co basin may be related to the  $N25^{\circ}W$  striking Jieze Caka fault. The latter displays normal slip as suggested by triangular facets observed in CORONA satellite imagery (Figure 14a). The Jieze Caka fault continues further to the west and changes strike to  $\sim N70^{\circ}W$  (Figure 12). The northern segment of the Xianqie Co fault zone continues to the northeast and links with an apparent west dipping transtensional fault. This range-bounding fault strikes  $\sim N10^{\circ}E$  and appears to control the location of the Lumajangdong Co basin (Figure 12).

[31] Left-slip kinematics along the Xianqie Co fault is indicated by CORONA satellite photographs that show a prominent south facing curvilinear fault scarp and associated left-slip displacement of a terrace riser (Figures 14c and 14d). Three different ages of terrace surfaces can be inferred based on the surface texture and albedo observed in the CORONA images (Figure 14d). They range from T3 for the ephemeral to active drainage, to T1 for the oldest terrace surface. The T1-T2 terrace riser displays a left-lateral offset of  $\sim 100$  m on the eastern side of the south-flowing stream (Figure 14c). The western terrace riser displays no apparent

offset, which we attribute to erosion by the active stream channel and which is consistent with left-slip motion.

### 3.3.2. Awong Co Fault System

[32] Located south of the Bangong-Nujiang suture zone is the Awong Co fault, which we interpret to be the strike-slip conjugate to the Xianqie Co left-slip fault (Figure 12). The range-bounding Awong Co fault strikes northwest and is curvilinear in map view. The northern segment of the Awong Co fault strikes  $\sim N65^{\circ}W$  and is sub parallel to the Bangong-Nujiang suture zone. However, to the south, the Awong Co fault becomes more oblique to the suture zone and strikes  $\sim N45^{\circ}W$ . Spatially corresponding to the change in fault strike are releasing bends as indicated by the location of Awong Co and Nier Co. This fault geometry suggests right-slip motion along the Awong Co fault. A north dipping thrust is shown in the map of Cheng and Xu [1987] juxtaposing Jurassic flysch over Cretaceous strata, which is truncated by the Awong Co fault (Figures 13a and 13b). We infer horizontal separation along the apparently active structure, however this inference does not preclude vertical motion. The magnitude of right lateral motion along the southern segment of the Awong Co fault is unknown.

## 4. Discussion

### 4.1. Kinematics of Active Deformation in Central Tibet

[33] The geologic observations presented above suggest that conjugate strike-slip faults are significant structures along the Bangong-Nujiang suture zone in central Tibet. Observations of strike-slip and normal faults near the Bangong-Nujiang suture zone are consistent with recently obtained fault-plane solutions of earthquakes in the region [Langin et al., 2001]. The presence of conjugate strike-slip faults along an elongate belt across central Tibet raises the question of their role, both in accommodating convergence between India and Asia in general, and specifically, their relationship to north trending rifts located north and south of the strike-slip systems. In the Qiangtang terrane, the left-slip faults are linked with NNE striking normal faults, as demonstrated along the Yibug Caka, Bue Co, and Aishi Co conjugate fault systems. In the Lhasa terrane, it has been long recognized that right-slip faults near the Bangong-Nujiang suture zone are kinematically linked with north trending rifts [Armijo et al., 1986, 1989] (Foldout 1 and Figure 1). Thus rifts in the Qiangtang and Lhasa terranes are kinematically linked by a series of conjugate sets of strike-slip faults in between. This mode of transferring extension is different from that along mid-ocean ridges where transform faults oriented perpendicular to normal faults is the rule. The difference may be explained by contrasting strain fields. Along the mid-ocean ridges, ridge-parallel compression is probably negligible. However, in Tibet rift-parallel (i.e., north-south) compression is significant as induced by the Indo-Asian collision.

[34] The presence of conjugate strike-slip faults in central Tibet is a refinement of the simple eastward extrusion model of a rigid Qiangtang [Armijo et al., 1989]. Our observations incorporate the left-slip faults of the Qiangtang, where the

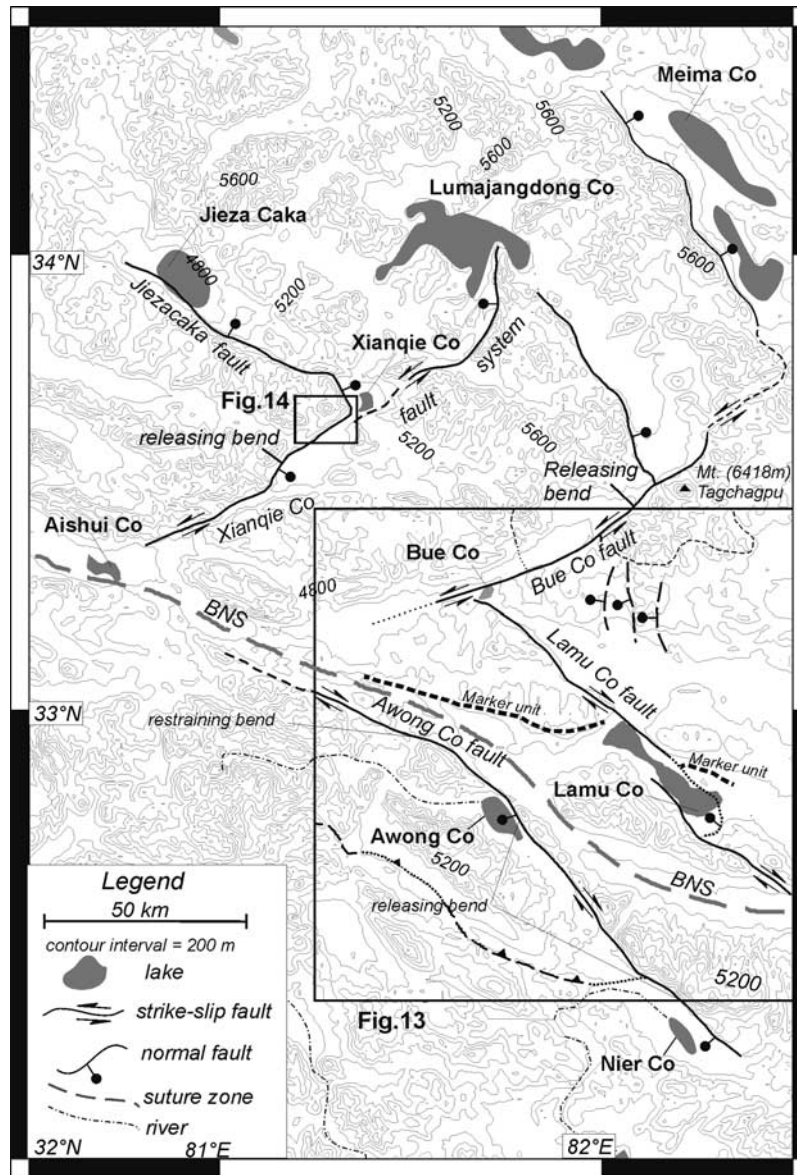


**Figure 12.** A simplified fault map showing the geometry of the Bue Co and Aishui Co conjugate strike-slip fault systems. See Foldout 1 for location.

conjugate strike-slip fault geometry together with the Tibetan rifts facilitates coeval north-south contraction and east-west extension. Because east-west extensional strain is distributed over central Tibet and is accommodated by the eastward extrusion of a series of small wedges bounded by conjugate strike-slip faults, the overall mode of east-west extension may be expressed as eastward “spreading” of the Tibetan plateau (Figure 15). Because the magnitude of strike-slip displacement is similar to a first-order for the active northeast and northwest striking strike-slip faults in central Tibet, we interpret this kinematic pattern to be suggestive of a constrictional strain, as originally postulated for Tibet by *Mercier et al.* [1987].

[35] Figure 15a is a schematic kinematic model for the active tectonics of central Tibet. The left-slip Kunlun fault in the north and the right-slip Karakorum-Jiali fault

zone in the south assist eastward spreading of Tibetan crust. To the east, crustal material turns toward the southeast and is bounded by the Ganzi-Xianshuihe-Xiaojiang fault system in the north and the Jiali-Red River fault system in the south. This kinematic pattern is consistent with the model of *Ratschbacher et al.* [1996] and recent GPS results from eastern Tibet [*Royden et al.*, 1997; *Chen et al.*, 2000].

[36] If fault-bounded blocks are rigid, conjugate strike-slip faulting along the Bangong-Nujiang suture zone would result in a gap at the trailing edge of the eastward moving wedge (Figure 16). The space may be closed by movement along east striking thrust faults (i.e., a trailing zipper), or by vertical-axis rotation of the surrounding rock mass and the strike-slip faults that bound the wedge-shaped block. Thrust earthquakes and folding in the late Cenozoic basins along

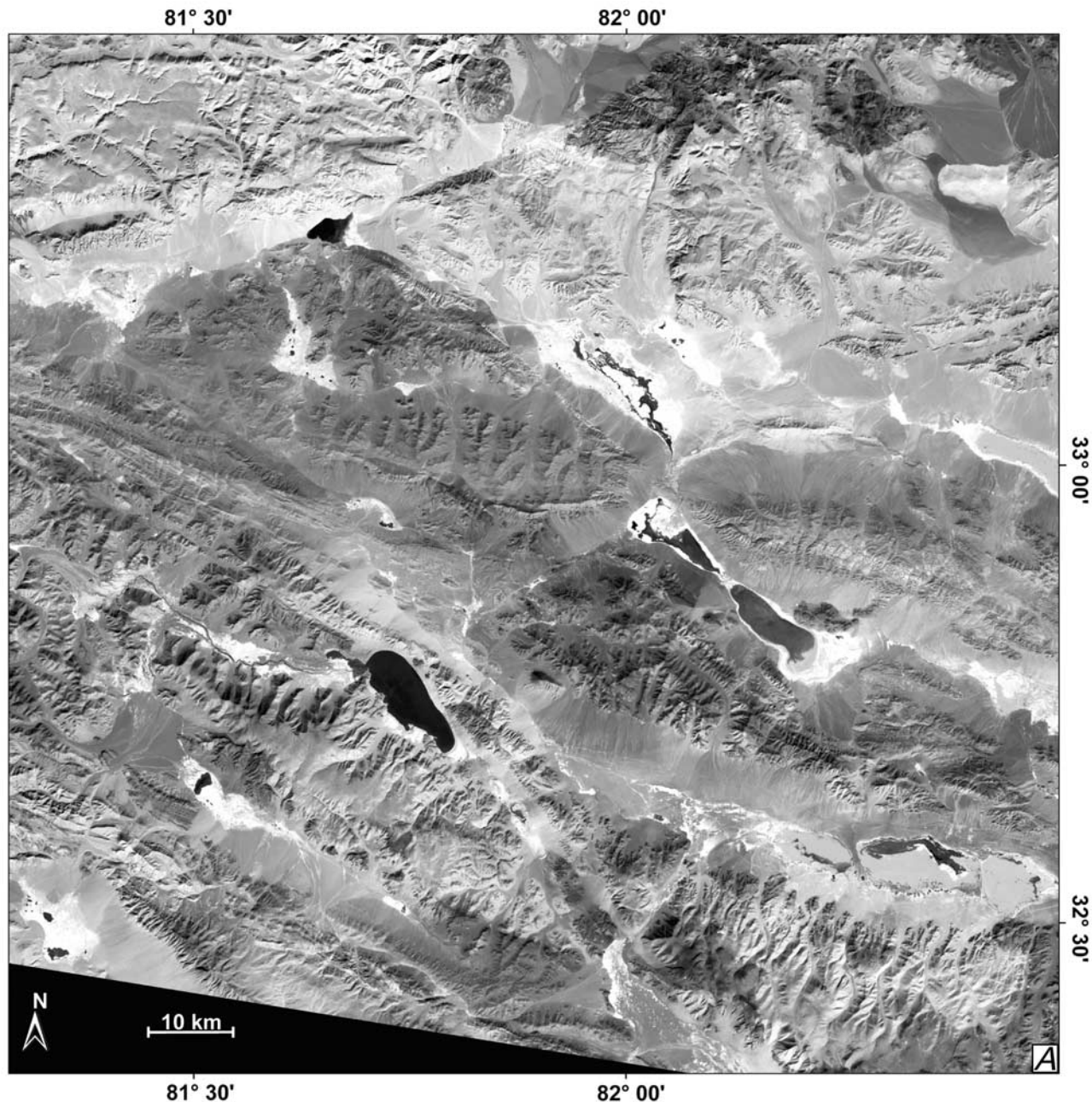


**Figure 13a.** Landsat-7 image was processed with an RGB color combination using channels 7-4-1. Note the prominent northeast and northwest striking faults. See Figure 12 for location and text for a discussion. See color version of this figure at back of this issue.

the Bangong-Nujiang suture zone would be expected with north-south contraction of the central Tibetan crust. However, this prediction is inconsistent with the absence of thrust earthquake mechanisms in central Tibet [Molnar and Lyon-Caen, 1989; Langin *et al.*, 2001] and the lack of east trending folds in the late Cenozoic strata along the Bangong-Nujiang suture zone based on our own field observations. Thus, we favor the geometry and kinematic pattern shown in Figure 16. This would explain the presence of numerous Quaternary basins such as the Siling Co, Lumpola, and Dong Co basins along the Bangong-Nujiang

suture zone (Foldout 1 and Figures 1 and 15). Perhaps the low elevation of the Bangong-Nujiang suture zone is induced by the extrusion of small crustal wedges bounded by conjugate strike-slip faults. Oblique-slip kinematics is predicted for the basin-bounding faults in this model.

[37] It has been postulated that major Cenozoic strike-slip systems in central Tibet reactivate older suture zones [Allègre *et al.*, 1984]. However, from field mapping, we found no evidence that the conjugate strike-slip faults in the central Tibet fault zone have been reactivated from older structures such as Mesozoic sutures and Tertiary thrusts.

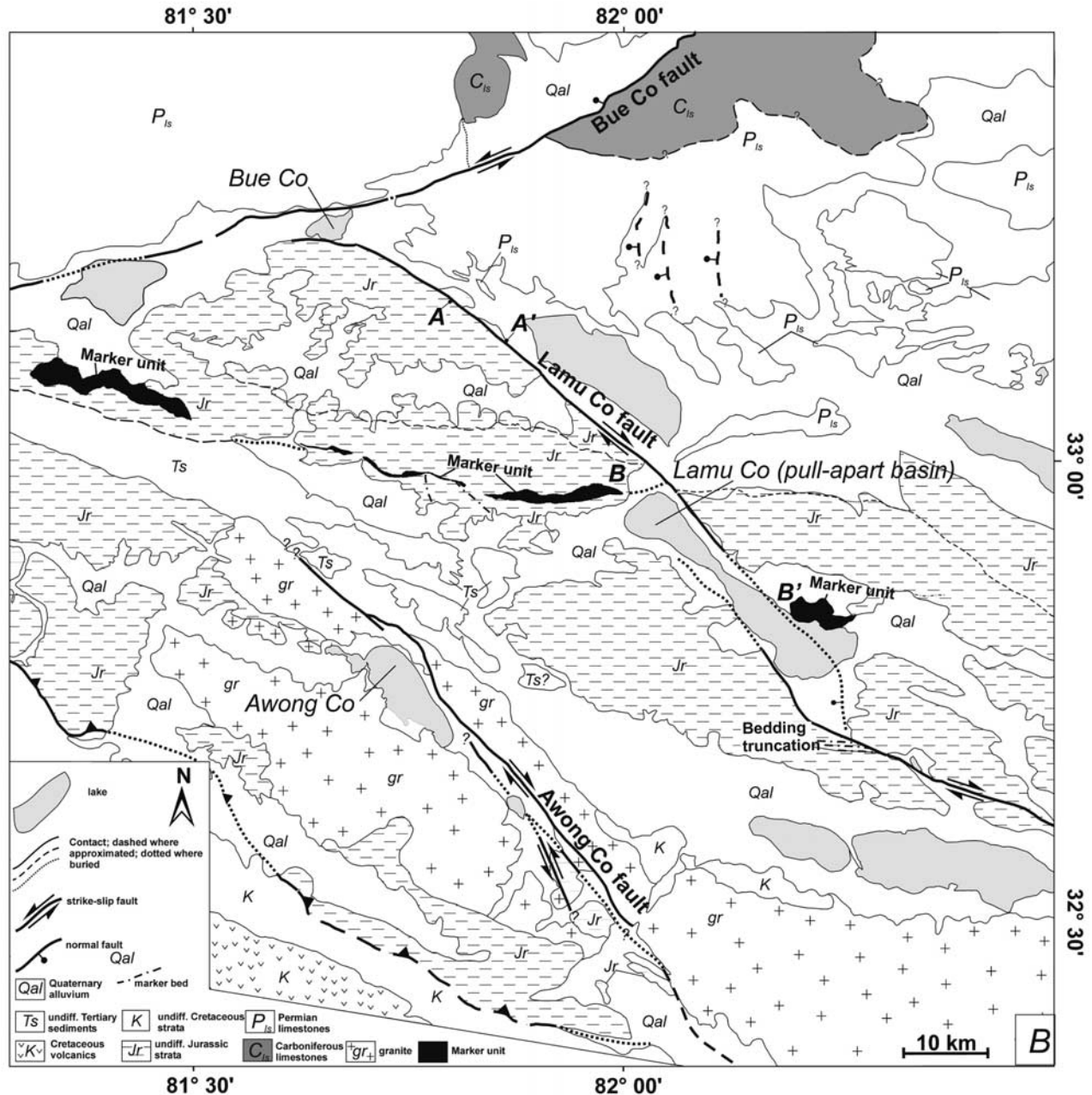


Figure 13b. Simple line drawing of geologic relationships shown in Figure 13a. A-A' and B-B' show a right separation of a distinct lithologic units. See text for a discussion.

Instead they consistently truncate and offset these older structures. If the strike-slip faults formed by the Coulomb fracture mechanism, their intersection angle across the east facing fault-bounded wedge should be about  $120^\circ$ , assuming a typical internal friction angle of  $30^\circ$ . However, the observed intersection angle between conjugate strike-slip faults is only  $\sim 70^\circ$ – $90^\circ$ . This implies that left-slip faults and fault-bounded blocks in the Qiangtang terrane may have rotated  $15^\circ$ – $25^\circ$  clockwise, whereas right-slip faults and fault-bounded blocks in the Lhasa terrane may have rotated  $15^\circ$ – $25^\circ$  counterclockwise. However, the magnitude of fault slip along the strike-slip faults is only  $\sim 12$  km, which

would be inconsistent with a predicted fault rotation of  $15^\circ$ – $25^\circ$ . Thus, we prefer a mechanism that includes a fault-bend fold mechanism on map view that would not require a large magnitude of fault rotation (Figure 16) [Peltzer and Tapponnier, 1988]. This prediction may be tested by future paleomagnetic studies.

#### 4.2. North-South Contraction and East-West Stretching of Central Tibet

[38] If we use 12 km as the average magnitude of strike-slip displacement along individual faults, a total of 12 km of

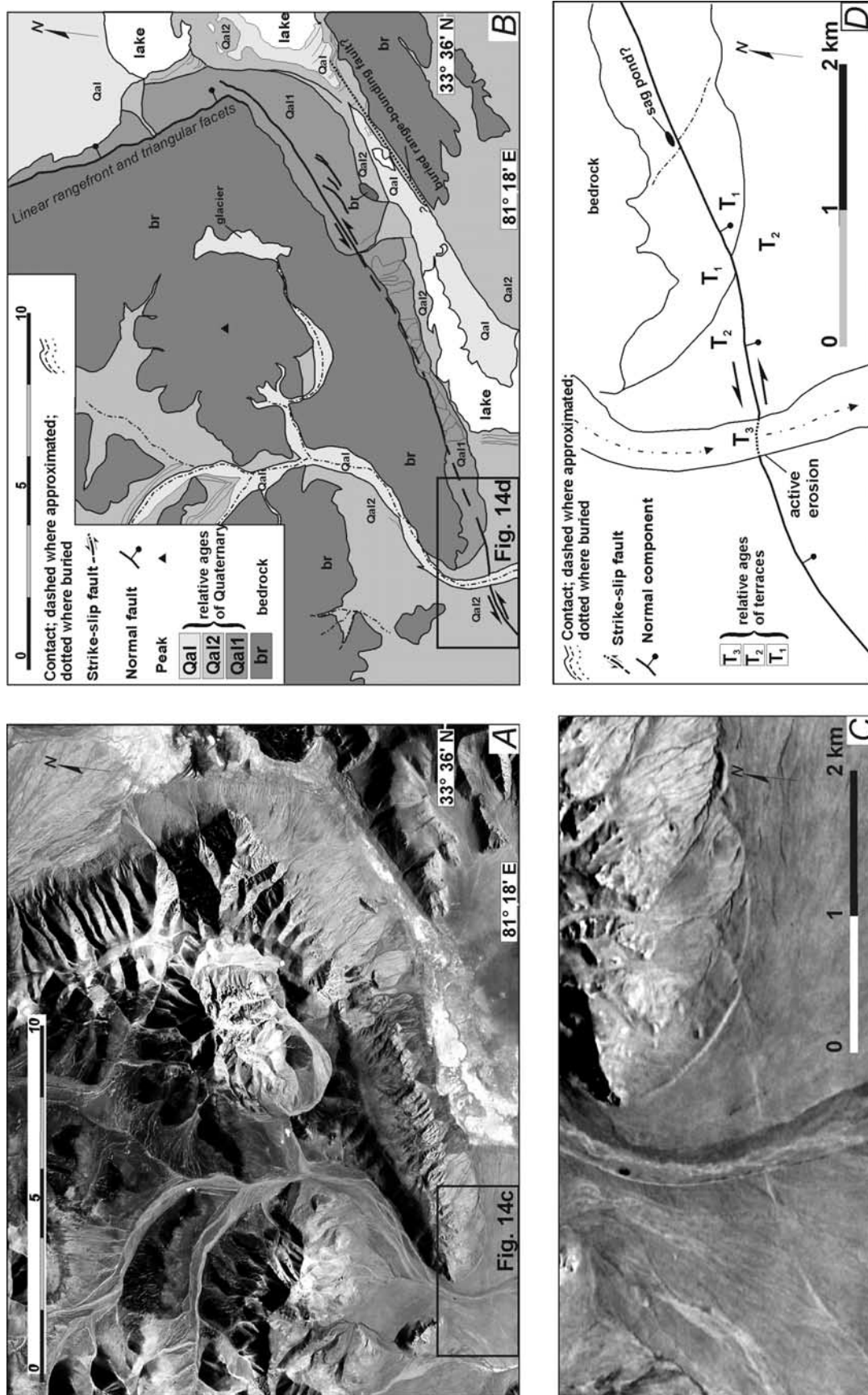


**Figure 14.** (a) CORONA image of the Xianjie Co fault. Note the conjoining fault segments comprised of the northeast striking Xianjie Co left-slip fault and a northwest striking normal fault that defines the range front. See Figure 12 for location. (b) Line drawing of key geologic relationships interpreted from the image shown in (a). (c) CORONA imagery showing left-slip displacement of a terrace riser along the Xianjie Co fault. (d) Interpretive line drawing showing key geologic relationships in (c). See (a) for location.

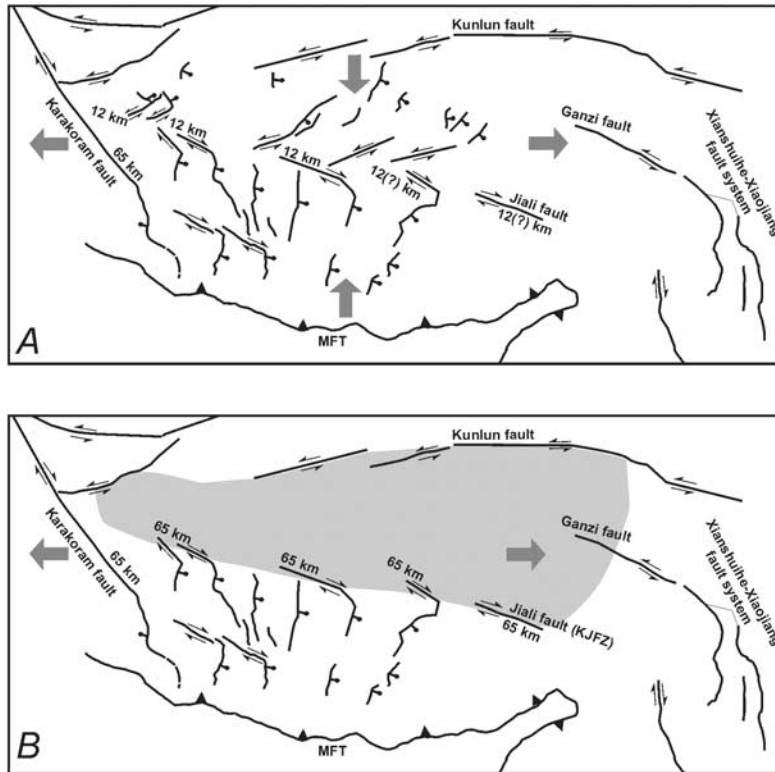


**Figure 15.** Schematic kinematic model of the active tectonics in central Tibet. (a) Conjugate strike-slip faults accommodate coeval east-west extension and north-south contraction in the interior of Tibet. Closely spaced (<150 km) conjugate strike-slip faults assist distributed eastward extrusion of small wedge-shaped blocks. (b) Alternatively, if rigid behavior of the Qiangtang terrane is correct, then a similar magnitude of slip along the Karakoram fault and the strike-slip faults that comprise the KJFZ is required.

north-south contraction should have been absorbed by motion on the conjugate left- and right-slip faults across the Bangong-Nujiang suture zone between  $31^{\circ}24'N$  and  $33^{\circ}30'N$  along the longitude of  $86^{\circ}E$ . Using the onset age of Tibetan rifts as a proxy for the initiation age of the kinematically linked conjugate strike-slip systems in central Tibet, which is between 14 and 8 Ma [Blisniuk *et al.*, 2001; Harrison *et al.*, 1995], the corresponding rates of north-

south contraction across the strike-slip fault zone are  $\sim 1-2$  mm/yr. This rate of contraction accounts for  $\sim 4\%$  of the Indo-Asian convergence rate if one assumes a total convergence rate of 37–47 mm/yr [Demets *et al.*, 1990; Gordon *et al.*, 1999; Shen *et al.*, 2000]. However, even the upper bound of our long-term rate is significantly lower than that determined by a GPS survey across the same range of latitude where our estimate was carried out. Although the

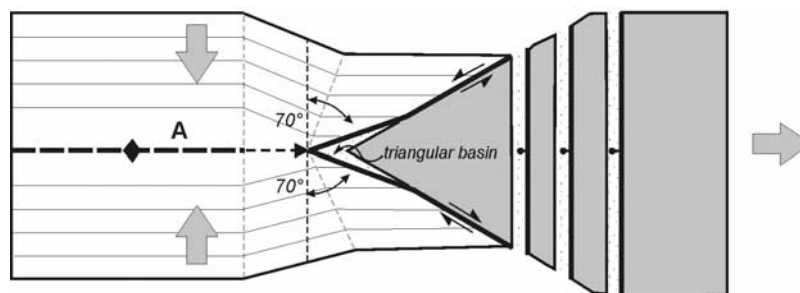


**Figure 16.** A potential interaction of conjugate strike-slip faults and related basin development at their intersection. The gap generated by the extruding wedge is closed by rotation of its surrounding rock mass, accompanied with minimal vertical axis rotations of strike-slip faults, and by rotation of its surrounding rock mass via the fault-bend fold mechanism, leaving a triangular basin at the tail end of the extruding wedge. Note distributed stretching of the extruding wedge.

uncertainties are large, the north-south contraction rate is  $5 \pm 3$  mm/yr as determined by the GPS survey of Wang *et al.* [2001]. This implies that the interior of Tibet may have accommodated an insignificant amount of north-south contraction on a timescale of millions of years than that determined by GPS studies on a timescale of several years.

[39] In comparison to the Karakoram fault, individual conjugate strike-slip fault systems in central Tibet display less finite strain by at least a factor of 5 (i.e., 12 km versus 65 km) [Murphy *et al.*, 2000]. The Altyn Tagh fault exhibits the largest displacement with  $\sim 500$  km of left-slip motion [Peltzer *et al.*, 1988; Yin and Harrison, 2000; Yin *et al.*, 2002]. However, the summation of eastward motion along the strike slip faults in central Tibet may be significant (Figure 15a). Specifically, integrating the east-west component of individual faults in this study accounts for  $\sim 33$  km of east-west stretching, which is more significant than north-south contraction by approximately a factor of 3. We suggest that this is likely a minimum estimate, as northeast and northwest striking strike-slip faults are present to the east and west of the study area presented in this paper. Thus, the magnitude of east-west stretching may be as high as  $\sim 60$  km if one includes slip along the Beng Co and Jiali strike-slip faults in east central Tibet, and the Longmu Co fault to the west (Foldout 1 and Figure 1). If our correlation is correct, it implies that the cumulative magnitude of east-west stretching across central Tibet could be of similar magnitude to the Karakoram fault. In turn, the Qiangtang terrane could not behave as a rigid block because, if this were the case, the magnitude of horizontal motion along individual faults (i.e., the Karakoram, Gyaring Co, Beng Co, and Jiali faults) [Armijo *et al.*, 1989] would each be  $\sim 65$  km (Figure 15b). When summed together, the total amount of eastward motion along the Karakoram fault and the central Tibet conjugate fault zone is at least  $\sim 125$  km.

[40] At a timescale of a few years, geodetic studies suggest that the slip-rate along the Altyn Tagh fault is  $\sim 10$  mm/yr or less [Bendick *et al.*, 2000; Shen *et al.*, 2001], and the long-term behavior of this structure suggests that it may slip at  $\sim 9$  mm/yr, which would be consistent with steady state behavior [Yin *et al.*, 2002]. A recent study of the intermediate-term behavior of the Karakoram fault suggests a relatively low slip rate along this structure at  $\sim 3$  mm/yr [Brown *et al.*, 2002]. In central Tibet a recent InSAR investigation suggests the southern segment of the Yibug Caka fault zone (i.e., the Riganpei Co fault) may be moving at a short-term rate that may be as high as  $\sim 5$  mm/yr [Taylor *et al.*, 2002].

## 5. Conclusions

[41] This study reveals a 200–300 km wide and 1500 km long east trending zone of conjugate strike-slip faults across central Tibet. The central Tibet conjugate fault zone consists of northeast striking left-slip faults north of the Bangong-Nujiang suture and northwest striking right-slip faults south of the suture. The conjugate faults merge toward the Bangong-Nujiang suture zone and accommodate coeval east-west extension and north-south contraction. Three conjugate fault sets in central Tibet were investigated. The Dong Co conjugate system adjacent to the central Bangong-Nujiang suture zone consists of the northeast striking left-slip Yibug Caka fault north of the suture and the northwest striking right-slip Gyaring Co fault south of the suture. The Bue Co and the Aishui Co conjugate systems are located along the western Bangong-Nujiang suture  $\sim 400$  km west of the Dong Co conjugate system. The Bue Co fault system consists of the northeast striking left-slip Bue Co fault in the north and the northwest striking right-slip Lamu Co fault in the south. The Aishui Co fault system consists of the northeast striking left-slip Xianqie Co fault in the north and the northwest striking right-slip Awong Co fault in the south. We use an average magnitude of horizontal fault motion of  $\sim 12$  km, as determined by offsets and separations of Tertiary thrusts and Paleozoic-Mesozoic lithologic units. This conjugate fault configuration requires a minimum of  $\sim 12$  km of north-south contraction and  $>31$  km of eastward extrusion to have been accommodated across the 200–300 km wide central Tibet conjugate fault zone. Because the conjugate strike-slip faults are kinematically linked with north trending Tibetan rifts that initiated between 14 and 8 Ma, our estimated magnitude of contraction implies a north-south contraction rate of  $\sim 1$ – $2$  mm/yr and  $>2$ – $4$  mm/yr of east-west extension across central Tibet. The presence of a series of conjugate fault systems in the interior of Tibet suggests that the central Tibetan crust has been spreading eastward via distributed eastward extrusion of small ( $<150$  km wide) wedge-shaped blocks.

[42] **Acknowledgments.** The National Science Foundation (EAR-98-05340), Geological Society of America, UC cooperative research program, Lawrence Livermore National Laboratory, and National Project for Research of the Tibetan Plateau (G1998040801) provided financial support. We thank Gary Axen, Stephanie Briggs, Eric Cowgill, Mark Harrison, Brian Horton, Carrie Menold, Mike Murphy, Gilles Peltzer, Alex Robinson, Paul Tapponnier, Alex Webb, and Jerome Van der Woerd, for thoughtful discussions of the Himalayan-Tibetan orogen. We thank Yong Zhou, Jessica D'Andrea, and Shundong He for their invaluable field assistance. Critical reviews by Kelin Whipple, Jean-Phillipe Avouac, and an anonymous reviewer helped clarify and improve the original manuscript.

## References

- Allègre, C. J., *et al.*, Structure and evolution of the Himalayan-Tibet orogenic belt, *Nature*, 307, 17–22, 1984.
- Armijo, R., P. Tapponnier, J. L. Mercier, and T. L. Han, Quaternary extension in southern Tibet: Field observations and tectonic implications, *J. Geophys. Res.*, 91, 13,803–13,872, 1986.
- Armijo, R., P. Tapponnier, and H. Tonglin, Late Cenozoic right-lateral strike-slip faulting in southern Tibet, *J. Geophys. Res.*, 94, 2787–2838, 1989.
- Arrowsmith, J. R., and M. R. Strecker, Seismotectonic range-front segmentation and mountain-belt growth in the Pamir-Alai region, Kyrgyzstan (India-Eurasia collision zone), *Geol. Soc. Am. Bull.*, 111, 1665–1683, 1999.
- Avouac, J. P., and P. Tapponnier, Kinematic model of active deformation in central Asia, *Geophys. Res. Lett.*, 20, 895–898, 1993.
- Avouac, J. P., J. F. Dobremez, and L. Bourjot, Paleoclimatic interpretation of a topographic profile across middle Holocene regressive shorelines of Longmu Co (western Tibet), *Paleogeogr. Paleoclimatol. Paleocol.*, 120, 93–104, 1996.
- Bendick, R., R. Bilham, J. Freymueller, K. Larson, and Yin Guanghua, Geodetic evidence for a low slip rate in the Altyn Tagh fault system, *Nature*, 404, 69–72, 2000.
- Blisniuk, P., B. Hacker, J. Glodny, L. Ratschbacher, S. Bi, Z. Wu, M. McWilliams, and A. Calvert, Normal faulting in central Tibet since at least 13.5 Myr ago, *Nature*, 412, 628–632, 2001.
- Brown, E. T., R. Bendick, D. L. Bourlès, V. Gaur, P. Molnar, G. M. Raisbeck, and F. Yiou, Slip rates of the Karakoram fault, Ladakh, India, determined using cosmic ray exposure dating of debris flows and moraines, *J. Geophys. Res.*, 107(B9), 2192, doi:10.1029/2000JB000100, 2002.

- Burchfiel, B. C., Z. Chen, L. H. Royden, Y. Liu, and C. Deng, Extensional development of the Gabor valley, southern Tibet, *Tectonophysics*, 194, 187–193, 1991.
- Cattin, R., and J. Avouac, Modeling mountain building and the seismic cycle in the Himalaya of Nepal, *J. Geophys. Res.*, 105, 13,389–13,407, 2000.
- Chen, Z., B. C. Burchfiel, Y. Liu, R. King, L. H. Royden, W. Tang, E. Wang, J. Zhao, and X. Zhang, Global positioning system measurements from eastern Tibet and their implications for India/Eurasia intercontinental deformation, *J. Geophys. Res.*, 105, 16,215–16,227, 2000.
- Cheng, J., and G. Xu, Geologic map of the Ritu region with report (in Chinese), 598 pp., Tibetan Bur. of Geol. and Miner Resour., Chengdu, People's Republic of China, 1987.
- Cogan, M. J., et al., Shallow structures of the Yadong-Gulu Rift, southern Tibet, from refraction analysis of Project INDEPTH common midpoint data, *Tectonics*, 17, 46–61, 1998.
- Coleman, M. E., and K. V. Hodges, Evidence for Tibetan plateau uplift before 14 m.y. ago from a new minimum age for east-west extension, *Nature*, 374, 49–52, 1995.
- Demets, C., R. G. Gordon, D. F. Argus, and S. Stein, Current plate motions, *Geophys. J. Int.*, 101, 425–478, 1990.
- Dewey, J. F., and K. Burke, Tibetan, Variscan and Precambrian basement reactivation: Products of continental collision, *J. Geology*, 81, 683–692, 1973.
- Dewey, J. F., R. M. Shackleton, C. Chengfa, and S. Yiyin, The tectonic evolution of the Tibetan Plateau, *Philos. Trans. R. Soc. London, Ser. A*, 327, 379–413, 1988.
- Edwards, M. A., and T. M. Harrison, When did the roof collapse? Late Miocene north-south extension in the High Himalaya revealed by Th-Pb monazite dating of the Khula Kangri granite, *Geology*, 25, 543–546, 1997.
- England, P., and G. Houseman, Extension during continental convergence, with application to the Tibetan plateau, *J. Geophys. Res.*, 94, 17,561–17,579, 1989.
- England, P., and P. Molnar, The field of crustal velocity in Asia calculated from Quaternary rates of slip on faults, *Geophys. J. Int.*, 130, 551–582, 1998.
- Garzone, C. N., D. L. Dettman, J. Quade, P. DeCelles, and R. F. Butler, High times on the Tibetan plateau: Paleoelevation of the Thakkola graben, Nepal, *Geology*, 28, 339–342, 2000.
- Gordon, R. G., D. F. Argus, and M. B. Heflin, Revised estimate of the angular velocity of India relative to Eurasia, *Eos Trans. AGU*, 80(46), F273, Fall Meet. Suppl., 1999.
- Harland, W. B., Tectonic Transpression in Caledonian Spitzbergen, *Geol. Mag.*, 108, 27–42, 1971.
- Harrison, T. M., P. Copeland, W. S. F. Kidd, and O. M. Lovera, Activation of the Nyainqen-tangla shear zone: Implications for uplift of the southern Tibetan Plateau, *Tectonics*, 14, 658–676, 1995.
- Kapp, P. A., Tectonic evolution of the Qiangtang terrane and the Bangong-Nujiang suture zone, central Tibet, 398 pp., Ph.D. thesis, Univ. of Calif., Los Angeles, 2001.
- Kapp, P. A., Y. Yin, C. E. Manning, T. M. Harrison, M. H. Taylor, and Lin Ding, Tectonic evolution of the early Mesozoic blueschist-bearing Qiangtang metamorphic belt, central Tibet, *Tectonics*, 22, doi:10.1029/2002TC001383, in press, 2003.
- Kidd, W. S. F., and P. Molnar, Quaternary and active faulting observed on the 1985 Academia Sinica-Royal Society Geotraverse of Tibet, *Philos. Trans. R. Soc. London, Ser. A*, 327, 337–363, 1988.
- Kong, X., and P. Bird, Neotectonics of Asia: Thin-shell, finite-element models with faults, in *The Tectonics of Asia*, edited by A. Yin and T. M. Harrison, pp. 18–35, Cambridge Univ. Press, New York, 1996.
- Langin, W. R., L. Brown, and E. Sandvol, Seismicity of Central Tibet from Project INDEPTH III seismic recordings, *Eos Trans. AGU*, 82(47), Fall Meet. Suppl., Abstract S31D-06, 2001.
- Lasserre, C., G. Peltzer, J. Van der Woerd, and Y. Klinger, Coseismic deformation from the  $M_w = 7.8$  Kokoxilli, Tibet earthquake, From ERS InSAR data, *Eos Trans. AGU*, 83(47), Fall Meet. Suppl., Abstract G61B-0987, 2002.
- Liao, K., (Ed.), Atlas of the Qinghai-Xizang Plateau, 237 pp., Inst. of Geogr., Sci. Publ. House, Beijing, 1990.
- Liu, Z., Geologic map of the Qinghai-Xizang Plateau, Geol. Publ. House, Beijing, 1988.
- Masek, J. G., B. L. Isacks, and E. J. Fielding, Rift flank uplift in Tibet: Evidence for a viscous lower crust, *Tectonics*, 13, 659–667, 1994.
- Mercier, J. L., R. Armijo, P. Tapponnier, E. Carey-Gailhardis, and T. L. Han, Change from Tertiary compression to Quaternary extension in southern Tibet during the India-Asia collision, *Tectonics*, 6, 275–304, 1987.
- Meriaux, A.-S., P. Tapponnier, F. J. Ryerson, J. van der Woerd, C. Lasserre, X. Xu, R. Finkel, and M. Caffee, Large-scale strain patterns, great earthquake breaks, and late Pleistocene slip-rate along the Altyn Tagh Fault (China), *J. Conf. Abstr. EUG*, 4(1), 55, 1999.
- Meyer, B. P., P. Tapponnier, L. Bourjot, F. Metivier, Y. Gaudemer, and G. Peltzer, Crustal thickening in the Gansu-Qinghai, lithospheric mantle-subduction and oblique, strike-slip controlled growth of the Tibetan plateau, *Geophys. Int.*, 135, 1–47, 1998.
- Molnar, P., and H. Lyon-Caen, Fault plane solutions of earthquakes and active tectonics of the Tibetan Plateau and its margins, *Geophys. J. Int.*, 99, 123–153, 1989.
- Molnar, P., and P. Tapponnier, Active tectonics of Tibet, *J. Geophys. Res.*, 83, 5361–5373, 1978.
- Murphy, M., A. Yin, T. M. Harrison, Ding Lin, and Guo Jinghui, Southward propagation of the Karakoram fault system, southwest Tibet: Timing and magnitude of slip, *Geology*, 28, 451–454, 2000.
- Owens, T. J., and G. Zandt, Implications and crustal property variations for models of Tibetan plateau evolution, *Nature*, 387, 37–43, 1997.
- Peltzer, G., and P. Tapponnier, Formation and evolution of strike-slip faults, rifts, and basins during the India-Asia collision: An experimental approach, *J. Geophys. Res.*, 93, 15,085–15,117, 1988.
- Peltzer, G., F. Crampe, and G. King, Evidence of nonlinear elasticity of the crust from the  $M_w$  7.6 Manyi (Tibet) Earthquake, *Science*, 286, 272–276, 1998.
- Ratschbacher, L., W. Frisch, G. Liu, and C. C. Chen, Distributed deformation in southern and western Tibet during and after the India-Asian collision, *J. Geophys. Res.*, 99, 19,917–19,945, 1994.
- Ratschbacher, L., W. Frisch, Changsheng Chen, and Guitang Pan, Cenozoic deformation, rotation, and stress patterns in eastern Tibet and western Sichuan, China, in *The Tectonics of Asia*, edited by A. Yin and T. M. Harrison, pp. 227–249, Cambridge Univ. Press, New York, 1996.
- Rothery, D. A., and S. A. Drury, The neotectonics of the Tibetan plateau, *Tectonics*, 3, 19–26, 1984.
- Royden, L. H., B. Burchfiel, R. King, E. Wang, Z. Chen, F. Shen, and Y. Liu, Surface deformation and lower crustal flow in eastern Tibet, *Science*, 276(5313), 788–790, 1997.
- Searle, M. T., Geological evidence against large-scale pre-Holocene offsets along the Karakoram Fault: Implications for the limited extrusion of the Tibetan, *Tectonics*, 15, 171–186, 1996.
- Searle, M. P., R. F. Weinberg, and W. J. Dunlap, Transpressional tectonics along the Karakoram fault zone, northern Ladakh: Constraints on Tibetan extrusion, in *Continental Transpressional and Trans-tensional Tectonics*, edited by R. E. Holdsworth, R. Strachan, and J. F. Dewey, *Geol. Soc. Spec. Publ.*, 135, 307–326, 1998.
- Searle, M. P., M. Asif Khan, J. E. Fraser, S. J. Gough, and M. Qasim Jan, The tectonic evolution of the Kohistan-Karakoram collision belt along the Karakoram Highway transect, North Pakistan, *Tectonics*, 18, 929–949, 1999.
- Shen, Z., C. Zhao, A. Yin, Y. Li, D. Jackson, P. Fang, and D. Dong, Contemporary crustal deformation in east Asia constrained by Global Positioning System measurements, *J. Geophys. Res.*, 105, 5721–5734, 2000.
- Shen, Zheng-Khang, M. Wang, Y. Li, D. Jackson, A. Yin, D. Dong, and P. Fang, Crustal deformation along the Altyn Tagh fault system, western China, from GPS, *J. Geophys. Res.*, 106, 30,607–30,621, 2001.
- Tapponnier, P., J. L. Mercier, R. Armijo, T. Han, and T. J. Zhao, Field evidence for active normal faulting in Tibet, *Nature*, 294, 410–414, 1981.
- Taylor, M., G. Peltzer, A. Yin, F. J. Ryerson, R. Finkel, and D. Lin, Active deformation in Central Tibet: Quantitative results from InSAR and geologic observations, *Eos Trans. AGU*, 83(47), Fall Meet. Suppl., Abstract T51B-1153, 2002.
- Van der Woerd, J., F. J. Ryerson, P. Tapponnier, A.-S. Meriaux, Y. Gaudemer, B. Meyer, R. Finkel, M. Caffee, Zhao Gouguang, and Xu Zhiqin, Uniform slip-rate along the Kunlun fault: Implications for seismic behavior and large-scale tectonics, *Geophys. Res. Lett.*, 27, 2353–2356, 2000.
- Van der Woerd, J., P. Tapponnier, F. J. Ryerson, A.-S. Meriaux, B. Meyer, Y. Gaudemer, R. C. Finkel, M. W. Caffee, and X. Zhiqin, Uniform post-glacial slip-rate along the central 600 km of the Kunlun fault (Tibet), from  $^{26}\text{Al}$ ,  $^{10}\text{Be}$ , and  $^{14}\text{C}$  dating of riser offsets, and climatic origin of the regional morphology, *Geophys. J. Int.*, 148, 356–388, 2002.
- Wang, Q., et al., Present-day crustal deformation in China constrained by global positioning system measurements, *Science*, 294, 574–577, 2001.
- Williams, H., S. Turner, S. Kelley, and N. Harris, Age and composition of dikes in southern Tibet: New constraints on the timing of east-west extension and its relationship to post-collisional volcanism, *Geology*, 29, 339–342, 2001.
- Wu, C., K. D. Nelson, G. Wortman, S. Samson, Y. Yue, J. Li, W. S. F. Kidd, and M. A. Edwards, Yadong cross structure and South Tibetan detachment in the east central Himalaya (89°–90°E), *Tectonics*, 17, 28–45, 1998.
- Yin, A., Mode of Cenozoic east-west extension in Tibet suggests a common origin of rifts in Asia during the Indo-Asian collision, *J. Geophys. Res.*, 105, 21,745–21,759, 2000.
- Yin, A., and T. M. Harrison, Cenozoic evolution of the Himalayan-Tibetan orogen, *Annu. Rev. Earth, Planet. Sci.*, 28, 211–280, 2000.
- Yin, A., T. M. Harrison, F. J. Ryerson, W. J. Chen, W. S. F. Kidd, and P. Copeland, Tertiary structural evolution of the Gangdese thrust system in southeastern Tibet, *J. Geophys. Res.*, 99, 18,175–18,201, 1994.
- Yin, A., P. A. Kapp, M. A. Murphy, T. M. Harrison, M. Grove, L. Ding, X. Deng, and C. Wu, Significant late Neogene east-west extension in northern Tibet, *Geology*, 27, 787–790, 1999a.
- Yin, A., T. M. Harrison, M. A. Murphy, M. Grove, S. Nie, F. J. Ryerson, X. F. Wang, and Z. L. Chen, Tertiary deformation history of southeastern and southwestern Tibet during the Indo-Asian collision, *GSA Bull.*, 111(11), 1644–1664, 1999b.
- Yin, A., et al., A Tectonic history of the Altyn Tagh fault system in northern Tibet inferred from Cenozoic sedimentation, *GSA Bull.*, 114(10), 1257–1295, 2002.

L. Ding, Institute of Geology and Geophysics, Chinese Academy of Sciences, Beijing 100029, People's Republic of China.

P. Kapp, Department of Geosciences, University of Arizona, Gould-Simpson Building, Tucson, AZ 85721, USA.

F. J. Ryerson, Institute of Geophysics and Planetary Physics, Lawrence Livermore National Laboratory, Livermore, CA 94550, USA.

M. Taylor and A. Yin, Department of Earth and Space Sciences, University of California, 3651 Geology Building, Los Angeles, CA 90095-156702, USA. (mtaylor@ess.ucla.edu)

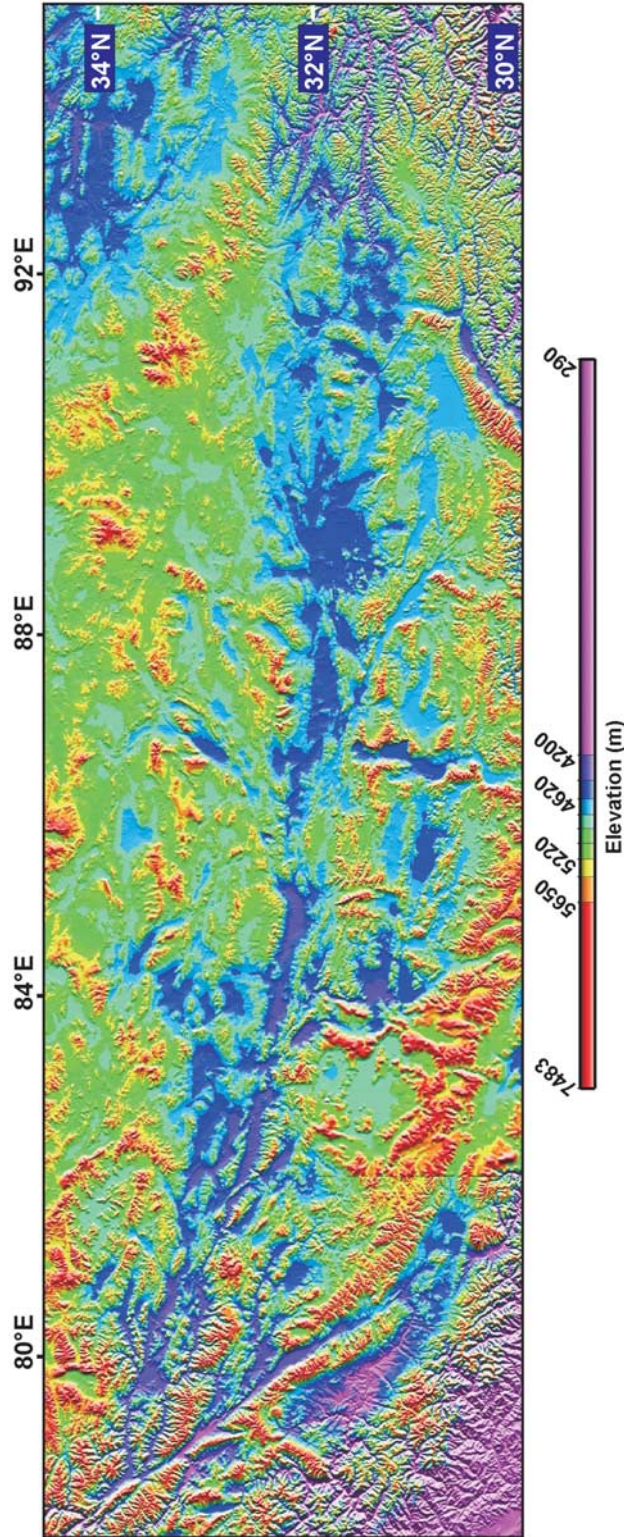


**Figure 1.** Color shaded relief map with a compressed palette of central Tibet showing a broad east-west trending depression (in dark blue) along the Bangong-Nujiang suture zone. Note that the depression is marked by a series of discontinuous basins. Strike-slip faults are represented by narrow and linear topographic structures trending northeast and northwest, north and south of the central depression. These linear features are the left-slip faults in the Qiangtang terrane and right-slip faults in the Lhasa terrane. Note that right-slip faults in the Lhasa terrane bound the northern margin of several north trending rifts, whereas left-slip faults in the Qiangtang terrane are connected with topographically less pronounced north trending rifts. The poor topographic definition of rifts in Qiangtang may result from the internally drained basin filling [Yin *et al.*, 1999b], or because of horizontal motion associated with strike-slip faulting.

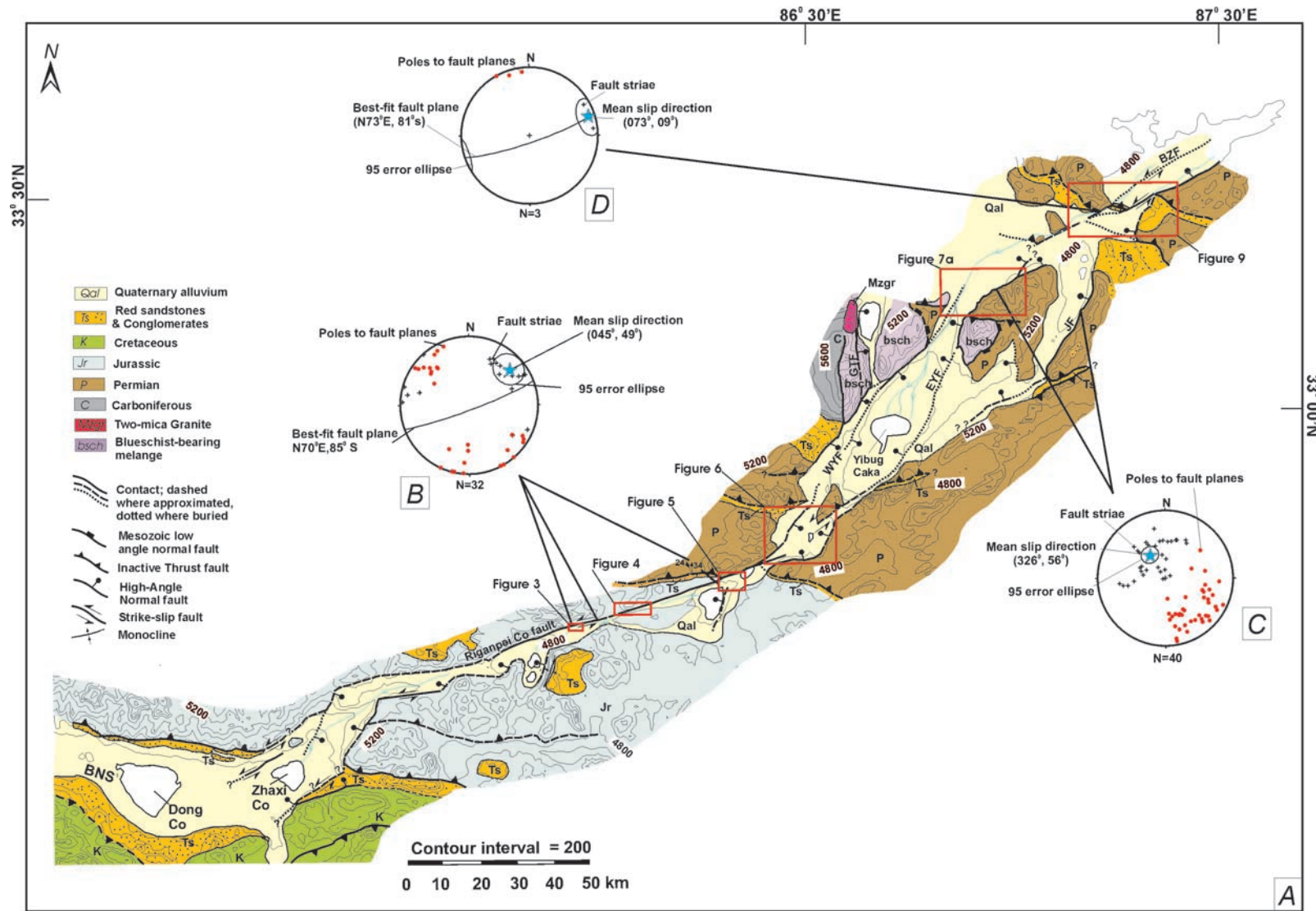


**Figure 2.** (a) Simplified tectonic map of the Yibug Caka fault zone, Qiangtang. (b), (c), and (d) are lower hemisphere stereographic projections of fault kinematic data. GTF = Gangtang fault, WYF = West Yibug Caka fault, EYC = East Yibug Caka fault, JF = Jiamou fault, BZF = Bu Zang Ai fault.

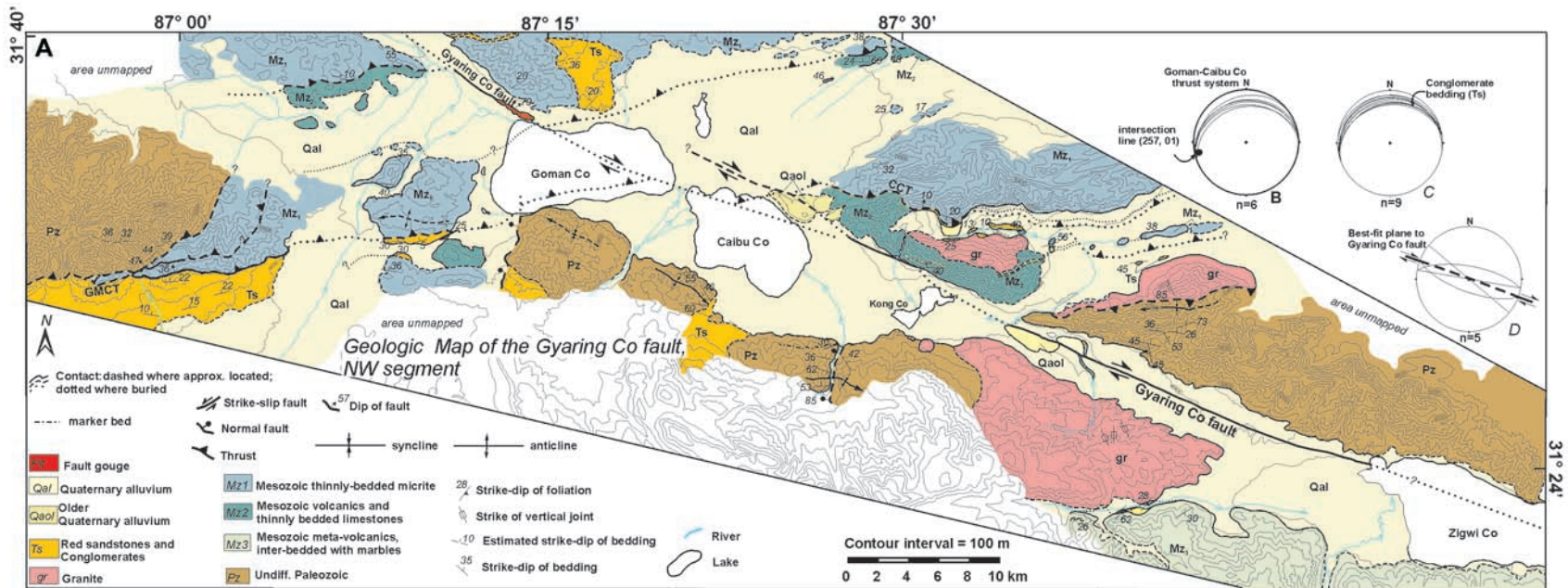


**Figure 10.** (a) Simplified geologic map of the northwest segment of the Gyaring Co fault located in the Lhasa terrane. See Foldout 1 for location. (b), (c), (d): Lower hemisphere, equal-area stereonet showing orientation data of the Goman-Caibu Co thrust faults, Tertiary unconformity, and the Gyaring Co fault used in the slip estimate of the Gyaring Co fault. GMCT = Goman Co thrust, CCT = Caibu Co thrust.

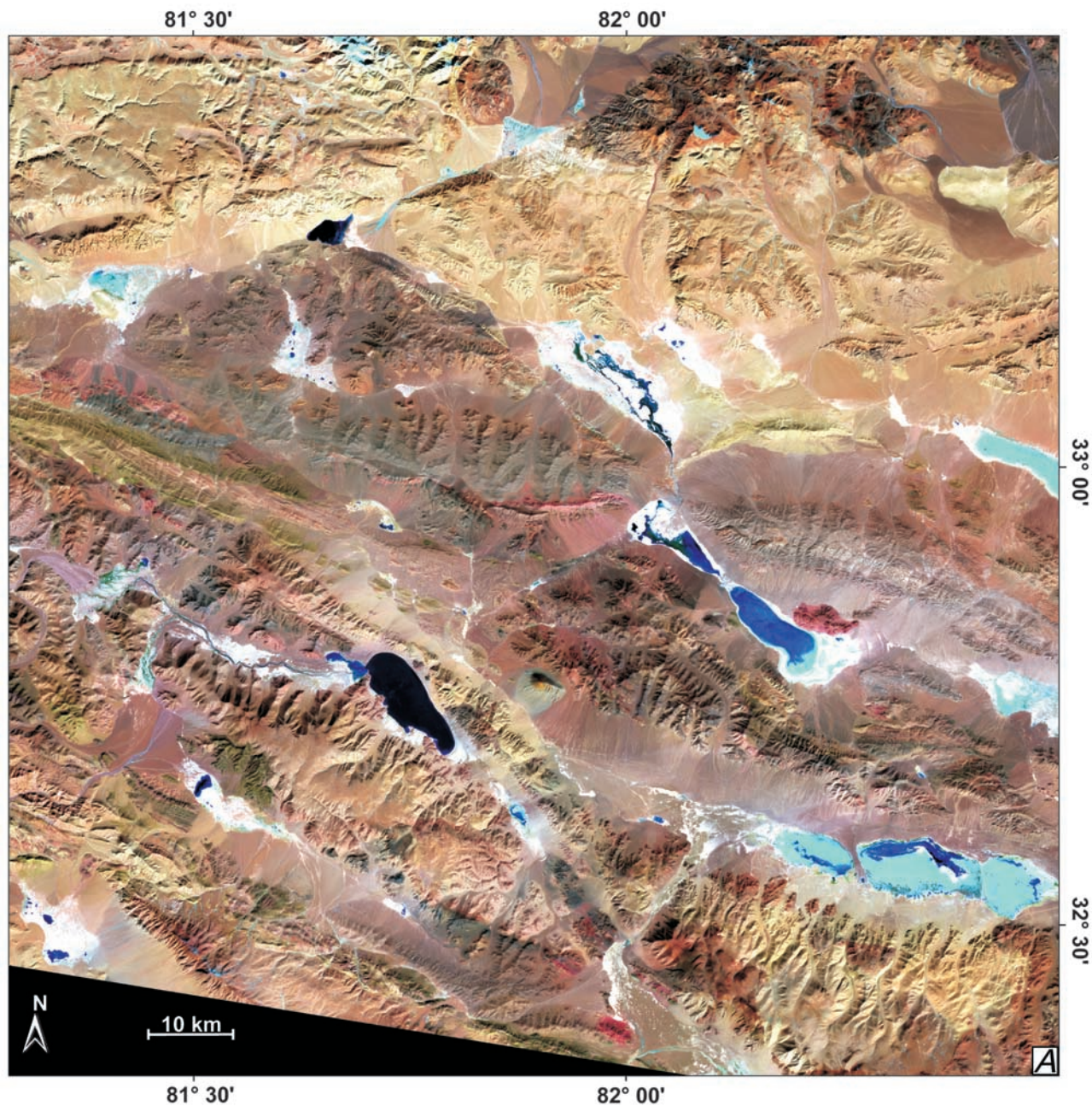


**Figure 13a.** Landsat-7 image was processed with an RGB color combination using channels 7-4-1. Note the prominent northeast and northwest striking faults. See Figure 12 for location and text for a discussion.